DALHOUSIE UNIVERSITY

THERMOBAROMETRY OF ECLOGITE FROM THE NORDØYANE ULTRA-HIGH PRESSURE DOMAIN, WESTERN GNEISS REGION, NORWAY

Benjamin Myrer

SUBMITTED IN PARTIAL FULFILLMENT OF THE REQUIREMENTS FOR
THE DEGREE OF BACHELOR OF SCIENCES, HONOURS
DEPARTMENT OF EARTH SCIENCES
DALHOUSIE UNIVERSITY, HALIFAX, NOVA SCOTIA

April 2020

DALHOUSIE UNIVERSITY

Department of Earth Sciences
Halifax, Nova Scotia
Canada B3H 4R2
(902) 494-2358

DATE: 03/30/2020

AUTHOR: Benjamin Myrer

TITLE: Thermobarometry of Eclogite from the Nordøyane Ultra-High Pressure Domain, Western Gneiss Region, Norway

DEGREE: B. Sc. Honours Earth Sciences CONVOCATION: May YEAR: 2021

Distribution License

DalSpace requires agreement to this non-exclusive distribution license before your item can appear on DalSpace.

NON-EXCLUSIVE DISTRIBUTION LICENSE

You (the author(s) or copyright owner) grant to Dalhousie University the non-exclusive right to reproduce and distribute your submission worldwide in any medium.

You agree that Dalhousie University may, without changing the content, reformat the submission for the purpose of preservation.

You also agree that Dalhousie University may keep more than one copy of this submission for purposes of security, back-up and preservation.

You agree that the submission is your original work, and that you have the right to grant the rights contained in this license. You also agree that your submission does not, to the best of your knowledge, infringe upon anyone's copyright.

If the submission contains material for which you do not hold copyright, you agree that you have obtained the unrestricted permission of the copyright owner to grant Dalhousie University the rights required by this license, and that such third-party owned material is clearly identified and acknowledged within the text or content of the submission.

If the submission is based upon work that has been sponsored or supported by an agency or organization other than Dalhousie University, you assert that you have fulfilled any right of review or other obligations required by such contract or agreement.

Dalhousie University will clearly identify your name(s) as the author(s) or owner(s) of the submission, and will not make any alteration to the content of the files that you have submitted.

If you have questions regarding this license please contact the repository manager at dalspace@dal.ca.

Grant the distribution license by signing and dating below.

_____ _____

Name of signatory Date

Table of Contents

Table of Figures

Table of Tables

Abstract

Partial melting of subducted continental crust at ultra-high pressure (UHP) conditions may facilitate the exhumation of large UHP terranes like the Western Gneiss Region (WGR), Norway. During the Scandian phase of the Caledonian orogeny, the subduction of Baltica beneath Laurentia resulted in eclogite-facies metamorphism of the WGR from ca. 415-405 Ma. In the Nordøyane UHP domain, the hottest domain in the region, eclogite bodies hosted in migmatitc orthogneisses well exposed sections of Kvernholmen and Flemsøya. Direct evidence for UHP metamorphism includes the discovery of coesite-bearing eclogite from northern Flemsøya and from Harøya. While there is abundant evidence for melting of the host rocks during decompression, evidence that partial melting occurred at peak pressure and temperature (P-T) conditions has not yet been observed. By examining eclogites from the domain that appear least affected by retrogression, this study is designed to test the hypothesis that the peak P-T conditions recorded in the eclogite bodies overlap with the field where UHP melting is possible for the host rocks.

The eclogite-facies mineral assemblage comprises omphacite + garnet + biotite + orthopyroxene ± rutile ± zircon, locally overprinted by retrograde amphibole + plagioclase ± biotite ± orthopyroxene ± clinopyroxene$_2$, with symplectite present along omphacite-garnet grain boundaries. Inclusions of quartz are rare in garnet and coesite is absent in the studied samples. Garnet hosts inclusions of omphacite, rutile, zircon, apatite, orthopyroxene, and idioblastic biotite.

Fe-Mg exchange thermometry applied to garnet-clinopyroxene, garnet-biotite, and garnet-orthopyroxene pairs yielded a T range of ca. 800-950 °C at 30 kb, assuming $Fe^{2+} = Fe_{total}$, and 500-750 °C if Fe^{3+} is calculated stoichiometrically. The discrepancy in T estimates when using Fe^{2+} or Fe^{3+} is interpreted as an affect of retrograde diffusion, resulting in unreliable T results. The Zr-in-rutile thermometer yielded T of ca. 700-820 °C at 20 kb, and ca. 750-860 °C at 30 kb, and because rutile is less susceptible to retrograde diffusion, these temperatures are interpreted as reliable. Thermodynamic modelling done with bulk composition CB15-19, paired with the Zr-in-rutile thermometer, yielded the best P-T range for CB15-19 of ca. 800-820 °C and ca. 25-32 kb. The inferred P-T conditions overlap with the fluid-present melting range for UHP rocks, however, there is no evidence for fluid infiltration or in situ melting of the eclogite bodies at peak P-T conditions. It therefore seems unlikely that partial melting of the host rocks at peak

UHP conditions facilitated the exhumation of the subducted WGR crust in the Nordøyane domain.

Key words: Western Gneiss Region, Nordøyane domain, ultra-high pressure metamorphism, eclogite-facies metamorphism, thermobarometry, thermodynamic modelling

Acknowledgements

I would firstly like to thank my honours supervisor Rebecca Jamieson for all her guidance and support during this project. Without her encouragement, knowledge, and revisions, the completion of this project would not have been possible. I would also like to thank Luke Hilchie for our discussions over the past summer and the invaluable advice he has provided to me throughout the year. Dan Macdonald is acknowledged for all his help and training in the electron microprobe lab, as well as Mitchell Kerr from Saint Mary's University for his help with rock crushing. I extend my thanks to Djordje Grujic for his commitment to the honours class and for his expertise, and finally, to my friends in the Department of Earth Sciences.

Chapter 1: Introduction

1.1 Statement of Problem

Ultra-high pressure (UHP) metamorphism in various crustal terranes around the world has been a topic of wide research since the first discoveries of coesite and microdiamond, minerals indicative of pressure (P) > 25 kb, within eclogite-bearing metamorphic belts (Chopin, 1984; Smith, 1984). The Western Gneiss Region (WGR), Norway, is one of the largest and best studied UHP terranes (Wain, 1997; Terry et al., 2000; Terry and Robinson 2003, 2004; Tucker et al., 2004; Kylander-Clark et al., 2007; Hacker et al., 2010; Butler et al., 2013, 2015). While the UHP metamorphism of the region can be attributed to the subduction of Baltica beneath Laurentia, the mechanisms responsible for the exhumation of the region are still widely debated. Some authors have argued that extension of overlying crust was responsible for exhuming subducted Baltican basement (Andersen, 1998; Krabbendamn and Dewey, 1998; Johnston et al., 2007; Hacker et al., 2010; Butler et al., 2015), while others have suggested that exhumation was facilitated by partial melting of subducted crust at UHP conditions (Labrousse et al., 2011; Ganzhorn et al., 2014). The first hypothesis is supported by regional scale amphibolite-greenschist facies asymmetric shear structures and symmetrical extensional fabrics that separate Devonian-Carboniferous basin sediments in the hangingwall from footwall UHP eclogites (e.g., Anderson, 1998; Johnston et al., 2007). Evidence in support of the second hypothesis, if it exists, is largely obscured by extensive melting during decompression. This study is designed to test the partial melting hypothesis by examining eclogites from the Nordøyane domain that appear least affected by retrogression during exhumation to see if they record P-T conditions compatible with UHP melting. In the domain, the hottest and deepest area within the WGR (Terry et al., 2000b; Cuthbert et al., 2000), the study areas of Haramsøya and Flemsøya comprise migmatitic orthogneisses that host abundant eclogite bodies, the target of the study, which may record these peak metamorphic conditions.

1.2 Regional Geology of the Western Gneiss Region

The Western Gneiss Region (WGR), an area in the southwest of Norway, is an erosional window that exposes Baltican Proterozoic basement gneisses, subducted to high pressure (HP) and ultra-high pressure (UHP) conditions of ca. 30 kbar and 800 ℃, corresponding to depths of ca. 100 km (Terry et al., 2000; Terry and Robinson 2003, 2004; Butler et al., 2013; Bryden,

2017). The basement rocks are granitoid orthogneisses, dated between 1680-1650 Ma, cut by ca. 1500 Ma granites and 1450-950 Ma gabbros (Terry et al., 2000; Krogh et al., 2011; Gordon et al., 2013). During the Ordovician-Devonian Caledonian Orogeny, subduction of the Iapetus Ocean led to the emplacement of continental and oceanic allochthons over Baltican basement from ca. 425 to 400 Ma (Terry et al., 2000; Hacker and Gans, 2005; Carswell et al., 2006; Hacker et al., 2010; Corfu et al., 2014). The Scandian phase of this orogeny resulted in continental-continental collision between Baltica and Laurentia and subduction of the Baltican margin beneath Laurentia, resulting in widespread HP and UHP metamorphism (Tucker et al., 2004; Hacker et al., 2010). The WGR includes three UHP domains, the Nordfjord /Stadlandet, Sorøyane, and Nordøyane domains (Figure 1.1) (Root et al., 2005), which all contain coesite-bearing eclogite and other indications of UHP conditions (coesite pseudomorphs, microdiamonds, thermobarometry) (Terry et al., 2000; Hacker et al., 2010; Butler et al., 2013).

1.3 Purpose and Scope of Study

In the southwestern Nordøyane domain, eclogites in the study areas of Haramsøya and Flemsøya comprise a peak mineral assemblage of omphacite + garnet + biotite ± orthopyroxene ± rutile ± zircon. Using conventional geothermobarometric methods and thermodynamic modelling with Theriak-Domino, this study aims to estimate the peak pressure and temperature (P-T) conditions recorded by the eclogites. Eclogite was chosen as these rocks are more likely to record the peak conditions than their host rocks, which record amphibolite-facies conditions. These P-T results will be used to test the hypothesis that the peak conditions recorded in the eclogite bodies overlap with UHP melting range for eclogites and their host rocks. If the P-T conditions do overlap with the field of UHP melting, these results may have implications for the mechanisms responsible for the exhumation of the WGR, such as the partial melting hypothesis. The objectives for this research are as follows:

- To analyze the petrography of the eclogites.
- To obtain electron microprobe analyses from the eclogite-facies mineral assemblage.
- To use conventional thermobarometry and trace-element thermometry to determine P-T conditions from the eclogite-facies mineral assemblage.
- To construct an equilibrium phase diagram for a representative bulk composition using thermodynamic modelling in order to constrain the peak P-T conditions further.

- To investigate which thermobarometric methods are most robust for the given mineral assemblages.

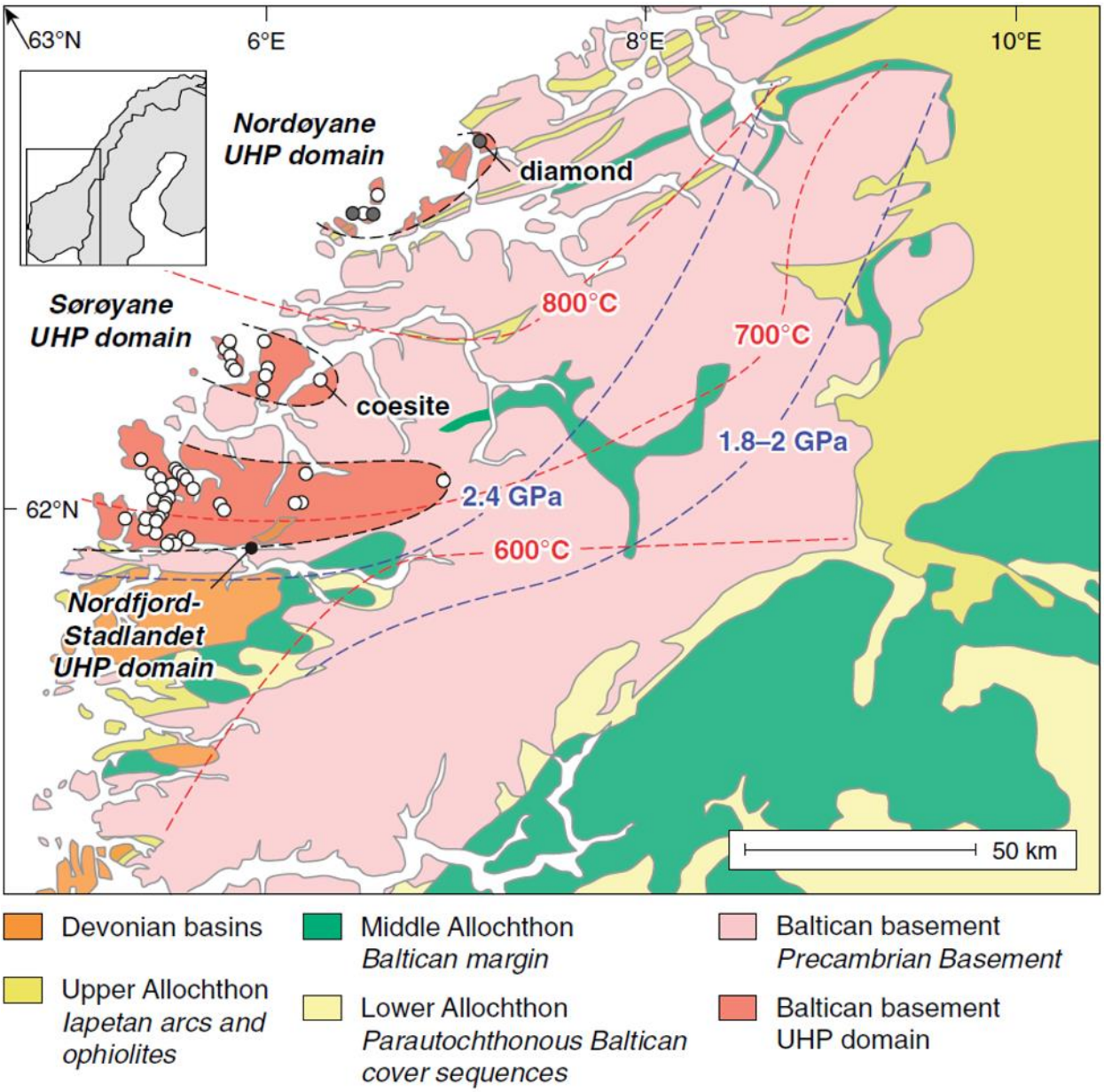

Figure 1.1: Geological map of the WGR, modified from Butler et al. (2015), showing the recognized UHP domains in red, the Nordfjord /Stadlandet, Srøyane, and Nordøyane domains. Dashed blue lines indicate peak pressures and red lines indicate peak temperature distributed within the region (Hacker et al., 2010). White dots show the discoveries of coesite/pseudomorph and grey cirlces show locations of microdiamond-bearing rocks.

Thermometry methods considered more robust (i.e. least susceptible to retrograde exchange effects), such as Zr-in-rutile trace-element thermometry, will be compared with Fe-Mg exchange thermometry between garnet and omphacite which is susceptible to retrograde cation exchange and unknown Fe^{3+}/Fe^{2+} values. Thermodynamic modelling will be used to determine P-T conditions independently and to provide an additional check on the reliability of conventional thermobarometry methods. The results presented will contribute to the overall understanding of the P-T conditions reached by eclogites and their host rocks in the Nordøyane domain, and whether melting could have occurred at these conditions. They may also have broader implications for the processes responsible for the exhumation of the WGR.

Chapter 2: Geological Setting

2.1 Geology of Nordøyane Domain

The Nordøyane UHP domain records the highest pressure and temperature conditions of the WGR of 3-5 GPa and 750-850°C (Terry et al., 2000; Cuthbert et al., 2000; Butler et al., 2013). Eclogite-facies metamorphism has been dated at 415-405 Ma, while amphibolite-facies metamorphism has been dated at 400-390 Ma (Terry et al., 2000; Krogh et al., 2011; Gordon et al., 2013; Butler et al., 2018). Terry and Robinson (2003, 2004) divided the domain into three separate segments, the Southern, Central, and Northern segments (Figure 2.1). While the segments vary in the metamorphic histories they record, they are all dominated by metamorphosed Baltica basement rocks which are infolded with amphibolites of the Blåhø Nappe and locally underlain by amphibolites of the Sætra Nappe (Terry et al., 2000; Terry and Robinson 2003, 2004). The Southern segment contains granitoid gneiss and local eclogite boudins that record HP, but not UHP conditions. The Central segment comprises granitic and intermediate gneisses with mafic dikes and lacks any eclogite, indicating that the unit may not have reached eclogite-facies conditions (Terry and Robinson, 2003, 2004; Butler et al. 2013). Separating the Northern and Central segments is the Åkre Mylonite, a major lower-amphibolite facies ductile structure (Terry et al., 2003). The Northern segment consists of migmatitic gneiss or augen orthogneiss, and migmatitic granodioritic to dioritic rocks with abundant eclogite boudins and is the only segment in the domain containing UHP eclogite (Terry and Robinson, 2003, 2004; Butler et al. 2013). The islands of Haramsøya and Flemsøya, the study locations of this research, are situated within the Northern segment (Figure 2.1); coesite has recently been discovered on northern Flemsøya (Hilchie et al., 2019).

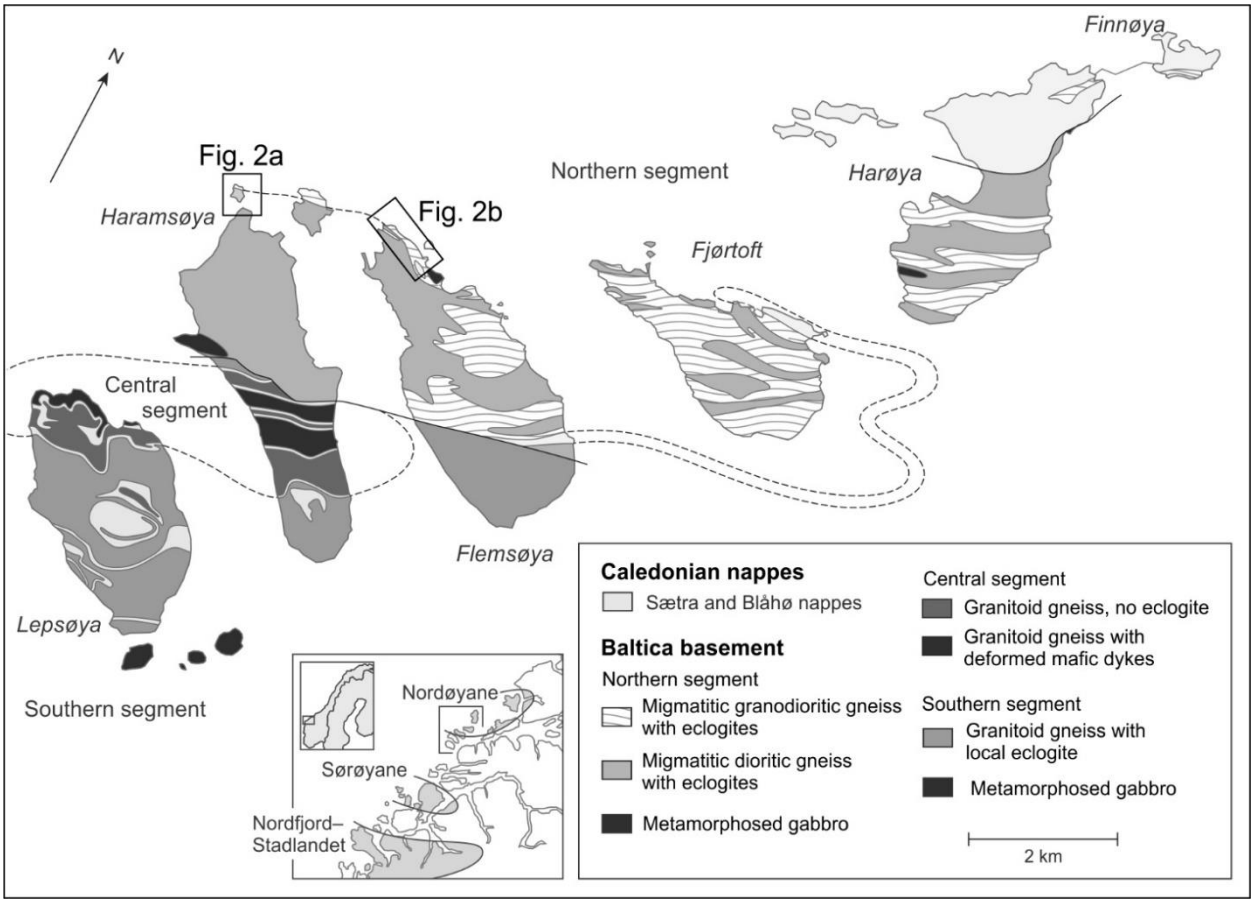

Figure 2.1: Simplified geological map of the Nordøyane domain, excluding the mainland (after Terry and Robinson, 2003; Butler et al., 2013, 2018). The study locations of Kvernholmen, on Haramsøya and the island of Flemsøya are indicated by boxes on the map (labelled Fig. 2a, 2b) (Modified from Butler et al., 2018) Inset shows location of UHP domains in western Norway.

Previous work in the area (Terry and Robinson, 2003, 2004) documented three distinct rock types in the Northern segment: Ulla gneiss, migmatitic gneiss, and augen orthogneiss. The Ulla gneiss underlies most of Haramsøya and is a garnet-biotite-hornblende gneiss containing coarse-grained eclogite boudins (Terry and Robinson, 2003, 2004). Migmatitic biotite – plagioclase – quartz ± hornblende gneiss- and K-feldspar augen orthogneiss with metamorphosed gabbro comprise the remainder of the Northern segment (Terry and Robinson, 2003, 2004). More recently, detailed mapping by Bryden (2017) on the northernmost Haramsøya and Flemsøya documented coarse scapolite pegmatites and scapolite-bearing migmatites and dioritic gneisses (Bryden and Jamieson, in press) and further subdivided the migmatitic units.

2.2 Geology of Study Area

Eclogite from the island of Kvernholmen, northern Haramsøya, and from the coast of Flemsøya between Skobergo and Seiholmen (Figure 2.2a, 2.2b) are the focus of this study. The following field descriptions are based on Bryden (2017) and Bryden and Jamieson (in press). Dioritic gneiss (Ulla gneiss) and augen gneiss comprise most of Kvernholmen (Figure 2.2a; Figure 2.3a,b), though granodiorites with abundant mafic enclaves host layered to massive eclogite bodies which range from 0.5 to 50 m across (Figure 2.3c). While many of the eclogite bodies have no preserved primary features, the variable proportions of omphacite, garnet, and biotite in the larger eclogite bodies define compositional layers, and the distribution of these bodies suggests that they are intrusions in the gneisses. Some larger eclogite bodies do display internal fabrics with steep lineations, locally truncated by fabrics in the orthogneisses (Terry and Robinson, 2004). Eclogite bodies smaller than 2 m across are typically massive and display extensive amphibolite-facies retrogression. On eastern Kverholmen, small eclogite bodies that are strongly lineated, called “pencil gneiss”, resemble eclogitised gabbros from other locations in the Northern segment and are interpreted as metagabbros (Terry and Robinson, 2004; Bryden and Jamieson, in press). The northeastern coast of Flemsøya comprises mainly K-feldspar augen gneiss with shallow-to-moderate- plunging lineations and locally, granodiorites with mafic enclaves and minor dioritic gneiss (Ulla gneiss) (Bryden and Jamieson, in press). Like Kvernholmen, eclogite bodies on the Flemsøya coast are situated in the granodiorites (Figure 2.3d) and the larger bodies display compositional layering defined by variable proportions of eclogite-facies minerals, enhanced by a generally strong foliation (Bryden and Jamieson, in press). In the study areas, grey dioritic to granodioritic selvages and dykes with mafic enclaves surround eclogite rafts (10-50 m) and similar material, previously interpreted as diatexite with schollen (e.g. Sawyer, 2008) is interlayered with orthogneisses.

2.3 Previous work on Nordøyane UHP Metamorphism

Evidence suggesting that the Nordøyane domain reached UHP conditions during metamorphism is considerable. Recently, coesite was reported from northern Flemsøya, a first for this part of Nordøyane (Hilchie et al., 2019). The enclave-rich granodiorite envelopes that surround many of the eclogite bodies are locally continuous with dioritic dykes that intrude some of the eclogite bodies (Hilchie et al., 2019). At Arhaugen on the north coast of Flemsøya, highly

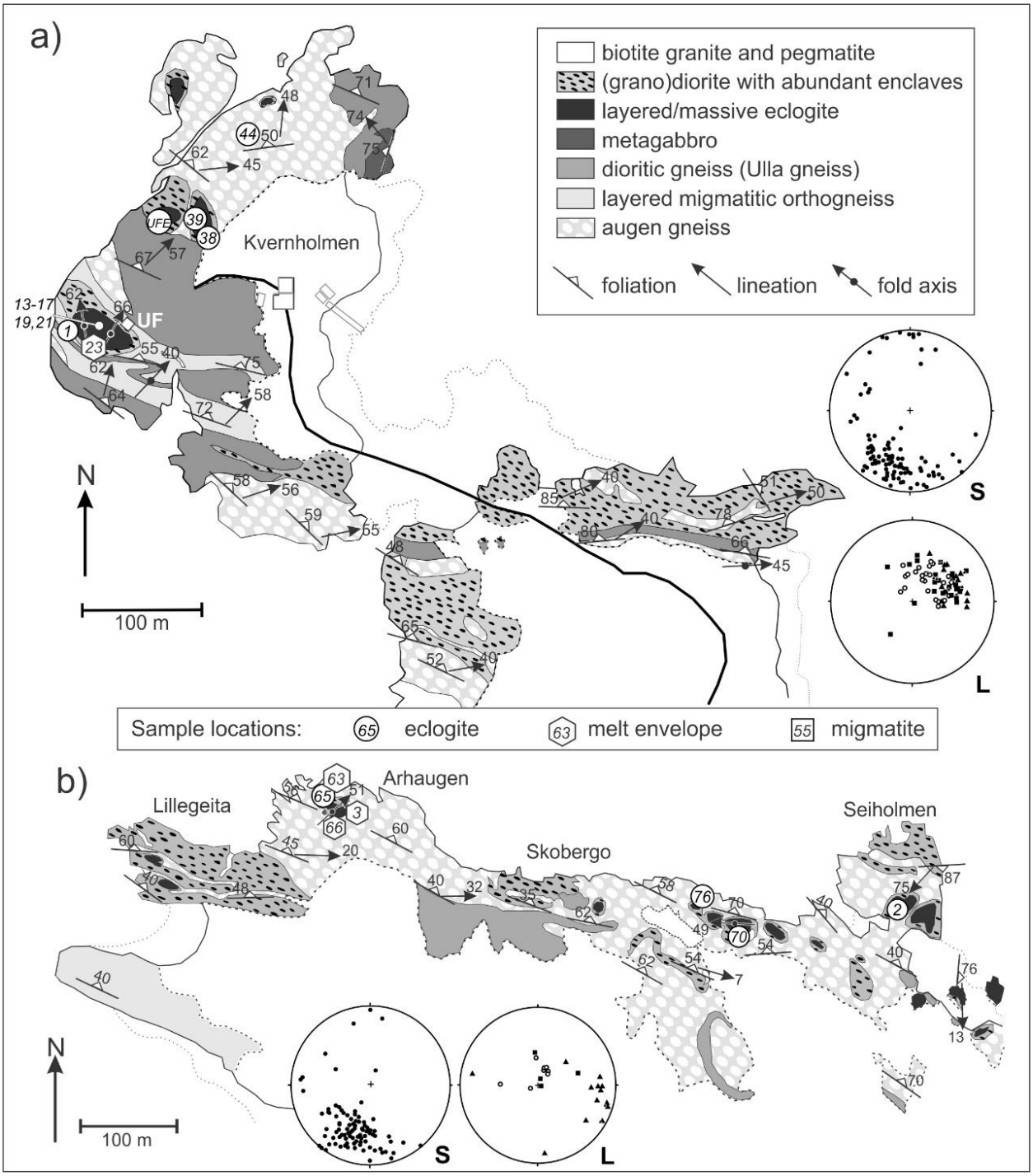

Figure 2.2. Geology of study area with sample locations (after Bryden & Jamieson, in press). a) Kvernholmen and adjacent mainland, northern tip of Haramsøya; UF = Ulla Fyr lighthouse. Samples 13-17, 19, 21 are eclogites from the Ulla Fyr body; CB15-19 is a major focus of this study. Sample CB15-44 was taken 200 m to the north. b) Arhaugen coastline, northeastern Flemsøya; sample CB15-70 located between Skobergo and Seiholmen. Light dotted lines indicate tidal range; dark dotted lines show limit of mapped outcrop. Insets show poles to foliations (S) and lineations (L) from each area (Bryden, 2017). Lineation data: open circles = eclogite facies lineations; squares = early linear fabrics in orthogneiss; triangles = amphibolite facies lineations.

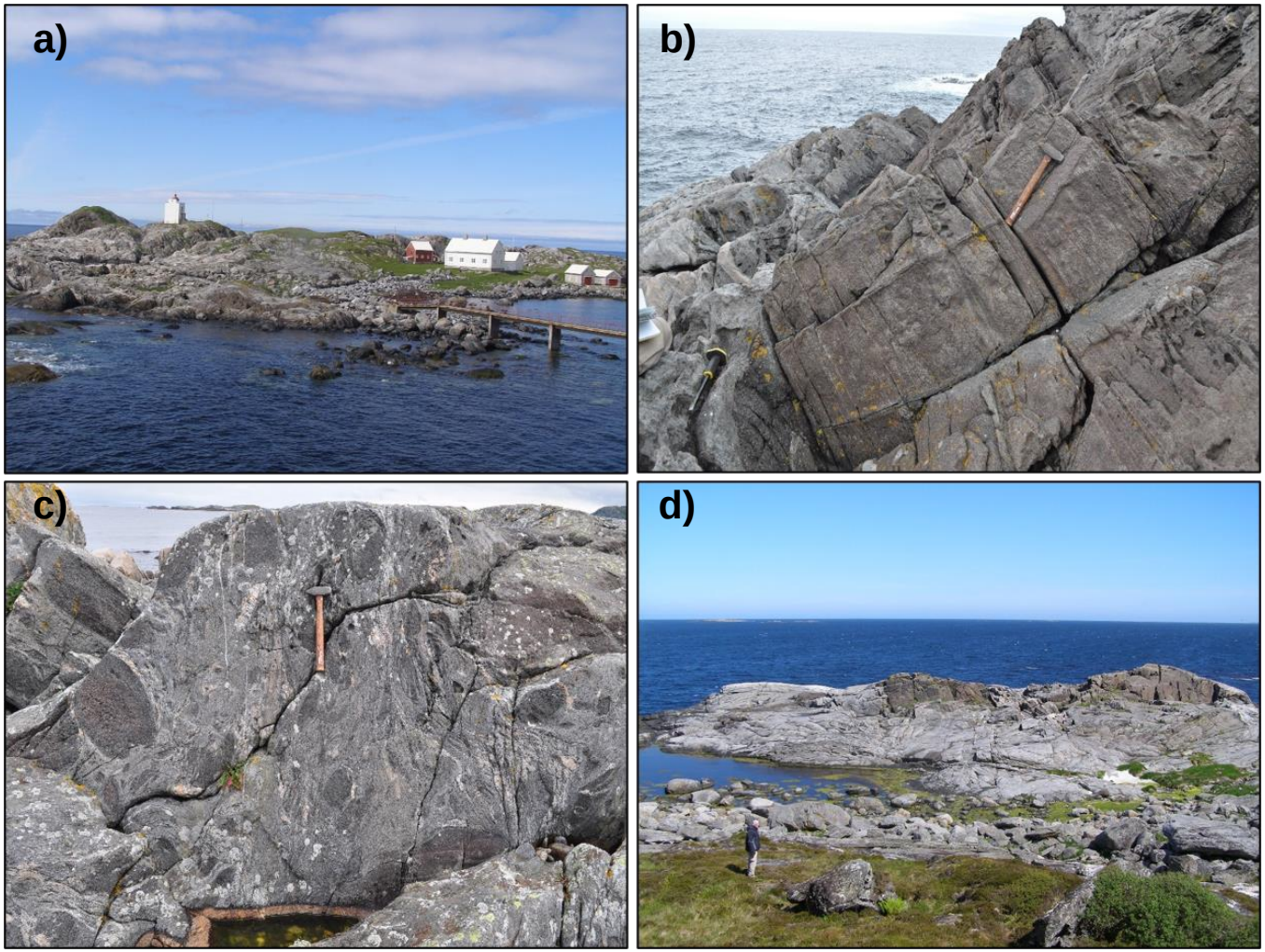

Figure 2.3. Field photos of study areas Kvernholmen and Flemsøya. a) island of Kvernhomen (looking to north) showing Ulla Fyr lighthouse. Ulla Fyr eclogite is large grey body to the west of the lighthouse. b) Large eclogite body west of Ulla Fyr lighthouse and site of sample CB15-19. View of contact between massive eclogite (upper right) and diorite selvage (lower left) c) Enclave-rich migmatitic diorite with amphibolitised eclogite fragments. d) Eclogite bodies east of Arhaugen; sample CB15-70 from south side of body (view is northeast; person as scale, ca. 1.8 m). Photos by G Chapman.

recrystalized eclogite bodies are separated from the adjacent granodiorite envelope by a dioritic dyke containing abundant xenocrysts of garnet and other eclogite-facies minerals (Hilchie et al., 2019). Garnet xenocrysts in the dyke and the granodiorite envelopes contain the coesite, as confirmed optically and by Raman spectroscopy (Hilchie et al., 2019). These coesite-bearing xenocrysts are texturally and compositionally different from garnets in adjacent eclogite bodies, indicating that they may have come from a different, maybe deeper, source (Hilchie et al., 2019; Jamieson et al., 2020).

Other direct evidence for UHP metamorphism in the Northern segment includes the discovery of microdiamond in garnet-biotite-kyanite gneiss and periodotite on northern Fjørtoft (Figure 1; Dobrzhinetskaya et al., 1995, Carswell et al., 2006). Subsequent thermobarometry on kyanite eclogites and kyanite-bearing eclogitized gabbro containing polycrystalline quartz pseudomorphs after coesite yielded P-T conditions of 820 °C at 30-36 kb (Terry et al., 2000). A maximum pressure of 3.8 GPa at 850 °C was recorded in orthopyroxene-bearing eclogites hosted within the basement gneisses from Fjørtoft (Carswell et al., 2006). Further evidence for UHP metamorphism came from the discovery of coesite-bearing eclogite from the island of Harøya, northeast of Fjørtoft (Butler et al., 2013), the first discovery of preserved coesite in the domain, yielding P-T conditions of ca. 3 GPa and 760 °C. U-Pb geochronology produced ages of ca. 415-410 Ma from metamorphic zircons in several Nordøyane eclogites (Krogh et al., 2011), and zircons from coesite eclogite on Harøya yielded a U-Pb age of 413 +/-6 Ma (Butler et al. 2018). Samples analyzed for this study come from Kvernholmen (CB15-19, CB15-44; Figure 2.2a; 2.3a) and the northeastern coast of Flemsøya (CB15-70; Figure 2.2b; 2.3d).

No detailed petrological study has yet been done on these rocks. Sample CB15-19, from a large eclogite body near the Ulla Fyr lighthouse (Fig. 2.2a; 2.3b), was chosen for analysis as it is texturally and compositionally homogenous. The sample comprises unzoned garnet grains, lacks a strong foliation, and appears to be well equilibrated. Sample CB15-70 displays clear compositional layering, preserves amphibolite-facies minerals in the matrix, and has experienced greater hydration than CB15-19; the sample comes from the coast of Flemsøya, between Skobergo and Seiholmen (Figure 2.2b). Sample CB15-44 is from a smaller eclogite body hosted in augen gneiss 200 m north of the Ulla Fyr lighthouse (Fig. 2.2a), is very coarse grained, and records more hydration than the other samples. Chapter 3 and Chapter 5 present the petrographic analysis of each sample and the thermobarometry results, respectively.

Chapter 3: Petrography

3.1 Introduction

Thin sections and hand samples of eclogite CB15-19, CB15-70, and CB15-44 from the Ulla Fyr and Flemsøya sections of the Nordøyane domain have been studied and the petrographic observations are presented in this chapter. While each sample has a typical eclogite facies mineral assemblage (garnet + omphacite), they were chosen to represent the variety of mineral assemblages and textural types present in the study area. The main textural differences include the absence or presence of foliations and the extent of retrogression in each sample, as evident from the degree to which symplectite is developed along grain boundaries, and the hydration of clinopyroxene to amphibole. CB15-19 is a massive, texturally homogenous, representative eclogite from the largest coherent eclogite body in the study area, Kvernholmen. The sample is relatively fresh with minor symplectite along grain boundaries and lacks evidence of retrograde hydration. CB15-70, from the Flemsøya section, was selected mainly because the sample is well foliated with compositional banding, comprising some layers largely replaced by symplectite and others that are relatively unaffected. CB15-44, from a smaller eclogite body north of Ulla Fyr, was chosen because of the abundant clinopyroxene-amphibole-plagioclase symplectite in the matrix and replacement of clinopyroxene by amphibole, indicating extensive retrogression. The sample also has very large garnet grains which host abundant inclusions.

3.2 Sample CB15-19

Sample CB15-19 is a massive, medium-grained eclogite consisting of ca. 40 modal % garnet, ca. 40% omphacite, 10-15% biotite, ca. 5-10% orthopyroxene, and 5% accessory phases including rutile, apatite, zircon, ilmenite, and rare quartz (Figure 3.1). The eclogite-facies assemblage is locally overprinted by retrograde amphibole + plagioclase ± biotite ± orthopyroxene ± clinopyroxene$_2$ (denoted $_2$ as it is different from and later than peak omphacite) ± carbonate minerals. Incipient clinopyroxene$_2$-amphibole-plagioclase symplectite can be seen along omphacite-garnet grain boundaries. Subidioblastic garnet is slightly elongated, ca. 0.5-2 mm in diameter, and contains randomly oriented inclusions of omphacite, rutile, zircon, apatite, orthopyroxene, and idioblastic (ca. 1 mm) biotite. Omphacite is subidioblastic to xenoblastic, ca. 0.5-1.5 mm, and like garnet, is elongated. Inclusions of rutile and biotite are present in omphacite, though sparse compared to the inclusions in garnet. Biotite in the matrix defines a

weak foliation and locally is associated with ilmenite. Characteristic UHP minerals such as coesite, kyanite, and phengite are not present in CB15-19. In this sample and the others analysed, quartz forms rare inclusions in garnet.

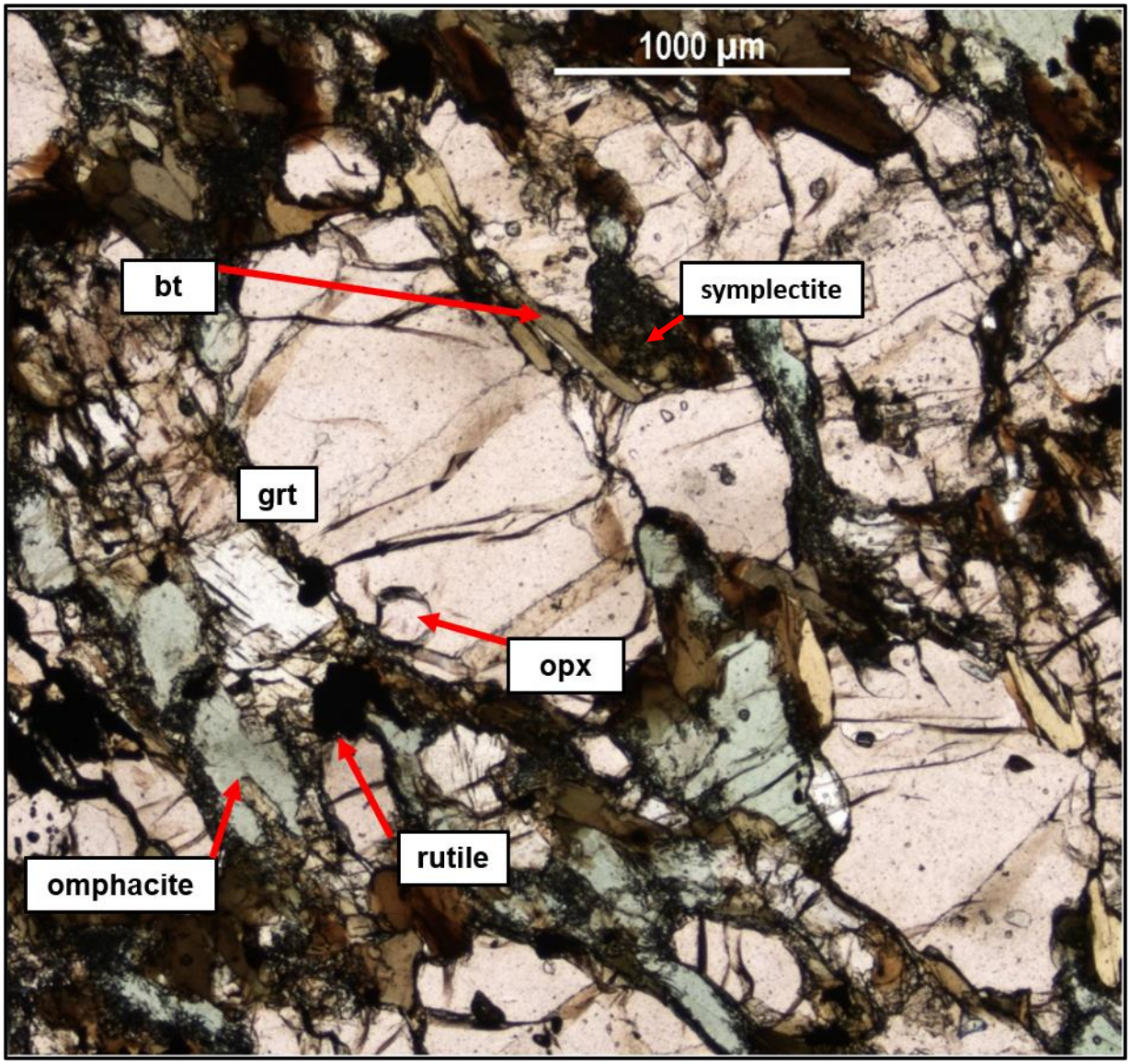

Figure 3.1. CB15-19, showing the interpreted peak mineral assemblage of garnet + omphacite + biotite + orthopyroxene. Symplectite texture is present along garnet and omphacite grain boundaries. (PPL; FOV = 6.25 mm)

Based on these observations, the peak eclogite-facies mineral assemblage is interpreted to be garnet + omphacite + biotite + orthopyroxene. Although biotite is not typical of UHP eclogites, it is considered to be part of the peak assemblage because it is present as abundant idioblastic inclusions in garnet, less commonly in omphacite, and has straight grain boundaries against these

minerals. Biotite inclusions are typically distributed in the cores of grains and are generally not spatially associated with fractures or embayments. Orthopyroxene is present as inclusions in garnet and as a stable phase in the matrix, however, locally is intergrown with biotite which suggests some late replacement.

3.3 Sample CB15-70

Sample CB15-70 is from an eclogite body on the north coast of Flemsøya (Fig. 2.2b), along-strike from sample CB15-19. The sample is well foliated and compositionally banded. It comprises a similar eclogite-facies assemblage to CB15-19, although some layers are extensively replaced by retrograde minerals. It contains 35-40 modal % garnet, ca. 10-15% orthopyroxene, ca. 30% omphacite, 10-15% biotite, and ca. 5% accessory phases (e.g. rutile, apatite, zircon, ilmenite) with compositional banding defined by layers dominated by clinopyroxene$_2$-amphibole-plagioclase symplectite and others consisting of coarse-grained garnet and omphacite (Figure 3.2a). The matrix is dominated by amphibole + plagioclase + biotite + orthopyroxene ± clinopyroxene$_2$, as well as symplectite that is coarser grained than in CB15-19, and minor carbonate. Similar to CB15-19, garnet and omphacite are elongated and help define the foliation (Figure 3.2b), however, the compositional banding is much stronger in CB15-70 and matrix biotite and secondary amphibole are more strongly aligned. Garnet is subidioblastic to xenoblastic, ca. 0.5-1.5 mm in diameter, and hosts inclusions of omphacite, orthopyroxene, biotite, rutile, ilmenite, apatite, and zircon. Xenoblastic omphacite is typically surrounded by symplectite and contains few inclusions of biotite and rutile. Orthopyroxene displayed a similar texture as omphacite and ranges from <0.5-1.0 mm across. The compositional banding is evident in hand sample and thin section, with layers of abundant symplectite up to 3 mm across alternating with well foliated layers of matrix amphibole, clinopyroxene$_2$, and biotite. Matrix biotite is commonly associated with coarse grained intergrown amphibole, indicating CB15-70 has experienced greater hydration than sample CB15-19. These intergrowths of amphibole and biotite, as well as clinopyroxene$_2$-plagioclase symplectite, have preferentially replaced pyroxenes. Amphibole is also quite common as an elongated matrix phase.

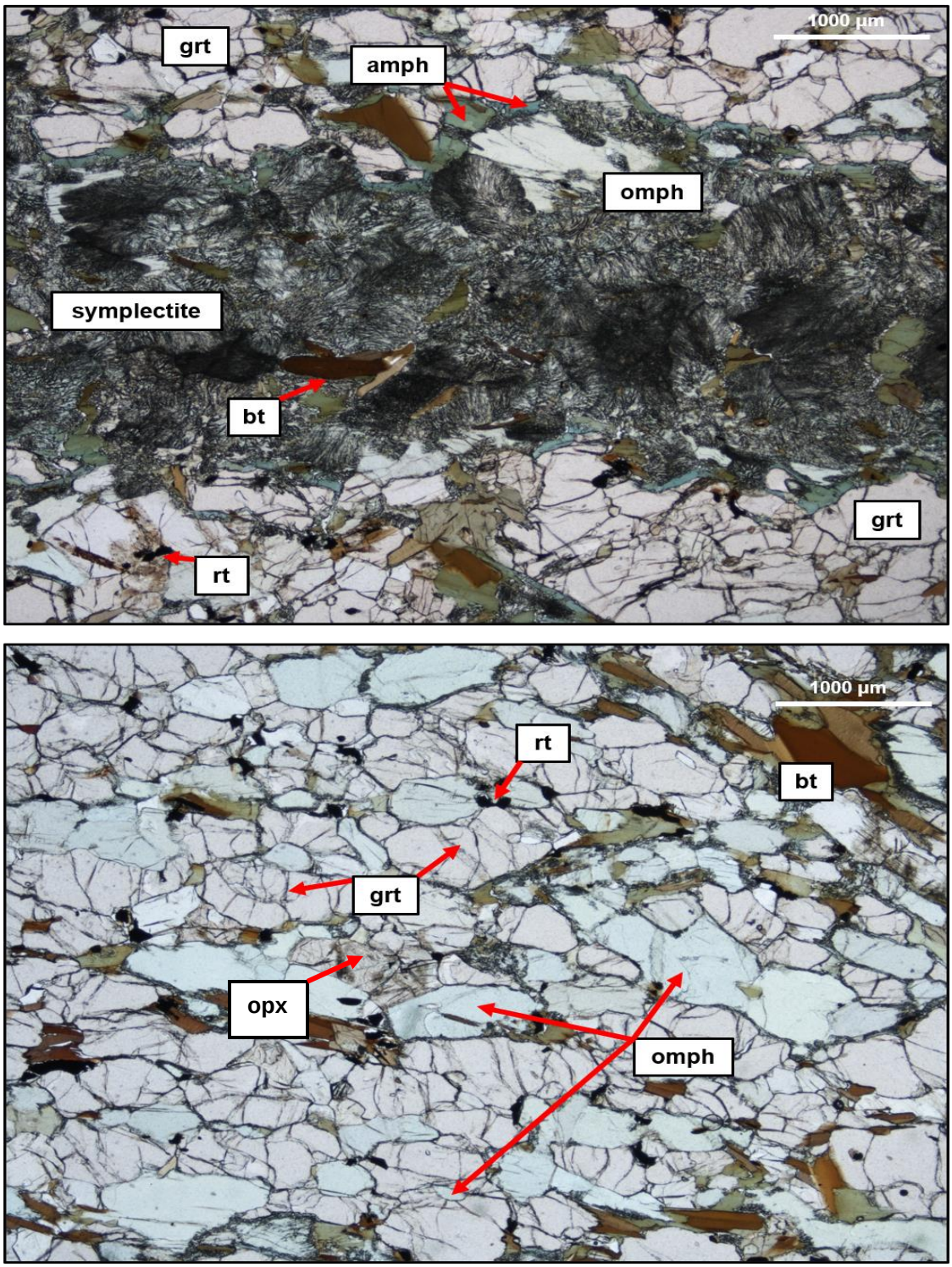

Figure 3.2. CB15-70. (a) Compositional banding defined by layers of matrix symplectite and coarser grained garnet and omphacite. (b) Peak assemblage of garnet + omphacite + biotite orthopyroxene (PPL; FOV= 6.25 mm)

Sample CB15-70 comprises a similar peak assemblage to CB15-19 of garnet, omphacite, orthopyroxene and biotite. Orthopyroxene is more abundant as inclusions in garnet in this sample compared to CB15-19 and represents a peak phase. Like CB15-19, biotite forms idioblastic inclusions in garnet and omphacite. It also defines a foliation with intergrown amphibole in the matrix and is interpreted to have been stable at both peak and retrograde conditions.

3.4 Sample CB15-44

CB15-44 is a massive, coarse-grained eclogite from a body north of CB15-19 on Kvernholmen. It is distinguished from CB15-19 and CB15-70 by the very coarse-grained garnet, the included assemblage in garnet, and the abundance of rutile and apatite, minor biotite, and well developed retrograde mineral assemblage. Garnet comprises 50-60 modal % of the sample, omphacite comprises 20-30%, biotite ca. 5%, and ca. 10-15% accessory phases such as rutile and apatite. The retrograde assemblage comprises orthopyroxene + clinopyroxene$_2$ + plagioclase + amphibole ± biotite, and clinopyroxene$_2$-amphibole-plagioclase symplectite (Figure 3.3a) is much more extensive than in the other samples. The most notable feature is the coarse-grained garnet which ranges from 5-10 mm in diameter (Figure 3.3b), at least 3 mm greater than garnet in CB15-19 and CB15-70. Xenoblastic garnet contains numerous inclusions of rutile, omphacite, apatite, zircon, zoisite, amphibole, ilmenite, biotite, titanite, and quartz, concentrated mainly in garnet cores. In comparison to the other samples, omphacite is small (ca. 0.5 mm) and sparse. Rutile is typically present as inclusions in garnet, but is also a matrix phase, ca. <0.5 mm across. Symplectite texture in the matrix varies from feathery and fine-grained to coarser-grained and vermicular and is more amphibole-rich than in other samples.

The peak mineral assemblage in this sample is harder to identify compared to CB15-19 and CB15-70 because of the extensive retrogression. The sample is dominated by retrograde phases such as biotite, amphibole, and clinopyroxene$_2$-amphibole-plagiolcase symplectite. Ilmenite in this sample is intergrown with very abundant rutile grains, biotite is less abundant (ca. <5%) than in the other samples, and orthopyroxene is absent. Garnet textures suggest that there may have been two phases of growth during peak and retrograde metamorphism. The presence of fresh omphacite inclusions is consistent with peak metamorphism, but the very coarse grain size and numerous inclusions of retrograde phases (e.g., amphibole) suggest a possible second phase of garnet growth.

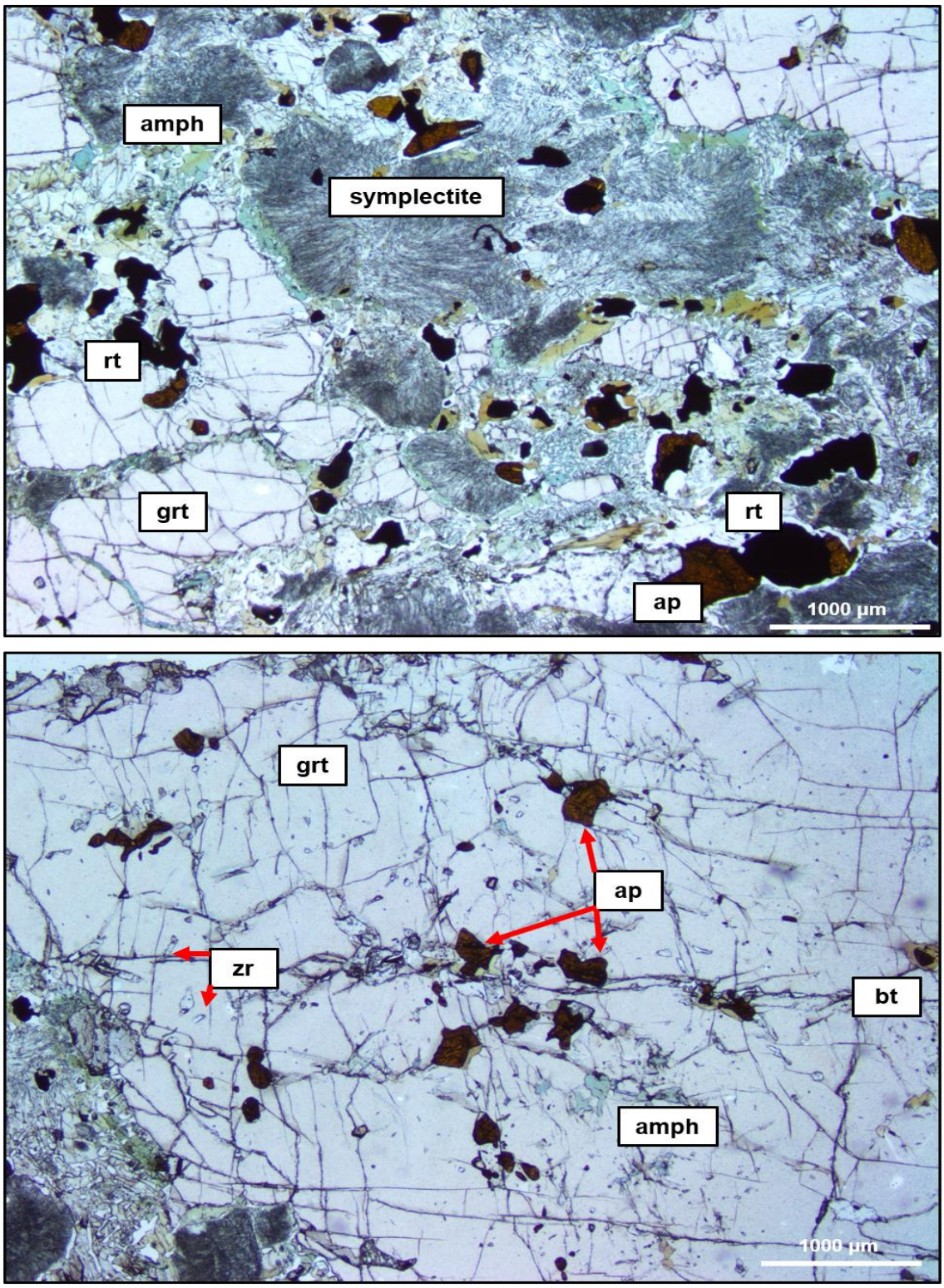

Figure 3.3. CB15-44. (a) Feathery matrix symplectite surrounded by amphibole. (b) Very coarse-grained garnet with inclusions of coarse apatite and amphibole. Smaller grains of zircon are distributed throughout. (PPL; FOV = 6.25 mm)

3.5 Petrographic Summary

Samples CB15-19 and CB15-70 have features in common, such as their peak and retrograde mineral assemblages, presence of omphacite, biotite, rutile, apatite, zircon, and orthopyroxene in garnet, and their similar grain sizes. Both samples have a foliation defined by elongated garnet, omphacite, and matrix phases such as biotite and clinopyroxene, though CB15-70 displays compositional banding and has a stronger foliation than CB15-19. Quartz is rare in both as an inclusion in garnet. Phengite, kyanite, and coesite documented in nearby UHP rocks are completely absent in all samples. Sample CB15-44 is distinguished from samples CB15-19 and CB15-70 by the abundant symplectite in the matrix, as well as the coarse-grained, 5-10 mm in diameter garnets and the titanite and zoisite inclusions in garnet. The compositional banding comprising alternating layers of the specified minerals is unique to CB15-70, though is quite common in other samples within the study areas. The textural homogeneity and massive texture distinguish CB15-19 from CB15-44 and CB15-70, and it is therefore interpreted to represent a fresh, more pristine eclogite than the others.

Chapter 4: Methods

4.1 Introduction

A major objective of this study is to determine the peak metamorphic pressure (P) and temperature (T) conditions of a selected sample of eclogites from the UHP Nordøyane domain, in the WGR of Norway, by employing conventional thermobarometry and thermodynamic software to plot calculated P-T estimates, and to calculate equilibrium phase diagrams (pseudo-sections). These samples comprise peak mineral assemblages of garnet + omphacite + biotite ± rutile ± orthopyroxene, and retrograde assemblages of clinopyroxene + plagioclase + amphibole + biotite ± orthopyroxene ± carbonate minerals.

4.2 Electron Microprobe Analysis

The JEOL JXA-2800 Superprobe in the Robert M. MacKay Laboratory at Dalhousie University was used to analyse the mineral compositions of the Nordøyane samples. The probe operated at a beam current of 20.0 nA and an accelerating voltage of 15.0 kV. Analysed elements included SiO_2, TiO_2, Al_2O_3, Cr_2O_3, FeO, MnO, CaO, Na_2O, and K_2O for anhydrous silicate minerals, with the addition of Cl and F for hydrous silicates. Rutile analyses included TiO_2, SiO_2, FeO, CaO, Al_2O_3, ZrO_2, V_2O_3, Nb_2O_5, Ta_2O_5, Cr_2O_3, and Y_2O_3. Full electron microprobe (EMP) analyses are presented in Chapter 5 and Appendix A and locations of analyses are presented in Appendix B.

In addition to mineral compositional data, back-scattered electron (BSE) images and wavelength dispersion spectrometry (WDS) X-ray maps were collected from areas selected for analysis. These images were used to select points for analysis and to assess compositional variations, including zoning, within grains of interest. Examples are given in Chapter 5.

4.3 Conventional Thermobarometry

4.3.1 Basic Principles

Conventional thermobarometry uses equilibrium thermodynamics, in combination with measured distribution coefficient, $K_D = (Fe^{2+}/Mg^{Grt})/(Fe^{2+}/Mg^{Cpx})$, values, to calculate pressure and temperature estimates from calibrations that have been established by natural and synthetic experiments (Powell & Holland, 2008). These calibrated thermometers are based on the interpreted equilibrium mineral assemblage in samples and the chemical reactions between these minerals during changes in P and T. The chemical reactions, including net transfer reactions and

ion exchange reactions, result in a change in mineral composition and/or assemblage which can be measured via EMP or other analytical techniques and the desired calibrated thermometer can be used to calculate P-T estimates (Powell and Holland, 2008).

In order to use mineral compositions as indications of metamorphic P-T conditions, conditions of equilibrium must first be presented. The stoichiometric relationship among components of phases in a chemical system can be described by the following expression:

$$0 = \sum_{j=1}^{m} v_j M_j \qquad \text{(eq. 4.1)}$$

which can also be written as an equivalent expression of the chemical potentials of those phase components:

$$0 = \sum_{j=1}^{m} v_j \mu_j \qquad \text{(eq. 4.2)}$$

where M_j is the chemical symbol for the j^{th} phase component, v_j is the stoichiometric coefficient of the j^{th} phase components in the reaction, and μ_j is the chemical potential of the j^{th} phase component and the summation is over all m phase components in the reaction (Spear, 1993). Using these equations, an expression for the equilibrium constant K_{eq} as a function of temperature and pressure can be derived (Spear, 1993), as follows:

$$\Delta G(P,T,X) = \Delta H(298.1) + \int_{298}^{T} \Delta C_P dT + \int_{1}^{P} \Delta V \, dP - T\left(\Delta S(298.1) + \int_{298}^{T} \frac{\Delta C_P}{T} dT\right) + RTlnK_{eq} = 0 \qquad \text{(eq 4.3)}$$

where ΔG is the free energy, ΔH is the enthalpy, ΔS is the entropy, ΔV is volume change, and ΔC_P is the heat capacity, all for the specified reaction (Spear, 1995). This is the fundamental equation used in thermobarometry with the goal of inferring the conditions at which a rock equilibrated by using the measured equilibrium constant to calculate T (at P) or P (at T). Most calibrated thermobarometers are based on a form of equation 4.3, modified for the specific reaction used.

Based on the silicate assemblages present, several Fe^{2+}-Mg exchange thermometers can be applied to the studied samples. These include the garnet-clinopyroxene thermometer (Ravna, 2000), the garnet-biotite thermometer (Holdaway, 2000), and the garnet-orthopyroxene

thermometer (Harley, 1984). The thermometers share several assumptions and limitations, which are discussed below using the garnet-clinopyroxene thermometer as an example.

4.3.2 Clinopyroxene-Garnet Thermometry

The first thermometer based on Fe-Mg exchange between clinopyroxene and garnet was proposed by Råheim & Green (1974). Their work presented the distribution coefficient, K_D between garnet and clinopyroxene which is a common variable to all clinopyroxene-garnet thermometers. The K_D should decrease with increasing T, and increase slightly with increasing P, though T-dependence is more sensitive than P-dependence (Råheim & Green, 1974). From their calibration, $T(°K) = \frac{3686+28.35\,P(kb)}{\ln K_D+2.33}$, they showed that the X_{Ca}^{Grt}, $X_{Ca}^{Grt} = \frac{Ca}{Ca+Mn+Fe^{2+}+Mg}$, had no effect on T estimates (Råheim & Green, 1974). Their experiments used a tholeiitic bulk composition and the results were applied to quartz eclogite. This thermometer has since been revised to account for compositional and other variables not considered in the original formulation (e.g., Ellis & Green, 1979; Ravna, 1988, 2000). Ellis & Green (1979) proposed a thermometer which sought to resolve inconsistencies in the work of Råheim & Green (1974), $T(°K) = \frac{3104\,X_{Ca}^{Grt}+3030+10.86\,P(kb)}{\ln K_D+1.9034}$. Their study introduced the effect of X_{Ca}^{Grt} on the K_D, showing that the reaction depends strongly on the grossular content of garnet. Other variables that are important for the various clinopyroxene-garnet thermometers include the magnesium number (Mg#), $X_{Mg\#}^{Grt} = \frac{Mg}{Mg+Fe^{2+}}$ and the mole fraction of spessartine, $X_{Mn}^{Grt} = \frac{Mn}{Ca+Mn+Fe^{2+}+Mg}$.

Ravna (2000) presented an updated calibration for the clinopyroxene-garnet thermometer based on a multiple regression analysis of experimental and natural datasets and compared the results to those based on previous calibrations (Raheim & Green, 1974; Ellis & Green, 1979; Ravna, 1988). Compared to the other thermometers discussed above, the results of this calibration indicated an improvement on the statistical relationships between T, P, X, and K_D. From analysis of 27 experimental datasets covering a large range of P and T conditions, and 49 natural high-Mn granulites, Ravna (2000) derived a widely applicable calibration, as follows:

$$T(℃) = [(1939.9 + 3270\,X_{Ca}^{Grt} - 1396\,(X_{Ca}^{Grt})^2 + 3319\,X_{Mn}^{Grt} - 3535\,(X_{Mn}^{Grt})^2 + 1105\,X_{Mg\#}^{Grt} - 3561\,(X_{Mg\#}^{Grt})^2 + 2324\,(X_{Mg\#}^{Grt})^3 + 169.4\,P(GPa))/(\ln K_D + 1.223)] - 273. \quad \text{(eq. 4.4)}$$

The reported uncertainty is ± 100 ℃ (Ravna, 2000).

The key improvements included corrections for $X_{Mg\#}^{Grt}$and X_{Mn}^{Grt}. Ravna (2000) noted that previous calibrations tended to overestimate T, and although including $X_{Mg\#}^{Grt}$ tends to underestimate temperature, a third-order polynomial function was introduced to correct for this. Ravna (2000) also showed that his own previous calibration (Ravna, 1988) underestimated T at X_{Ca}^{Grt} <0.20 and >0.45. After reviewing work done on Mn-rich systems and the effect of Mn in garnet-clinopyroxene thermometry (Bhattacharya et al.,1990), Ravna (2000) included X_{Mn}^{Grt} as a variable in the calibration, as omitting it (e.g., Ellis & Green, 1979) tends to underestimate T. These improvements make the Ravna (2000) calibration the most robust garnet-clinopyroxene thermometer for the Nordøyane eclogites.

4.3.3 Assumptions and Limitations

The most important limitation when using conventional thermobarometry is the need to assume that the mineral compositions recorded in the rocks reflect equilibrium. Criteria used to assess this include textural equilibrium (e.g., sharp grain boundaries between phases, lack of retrogression) and compositional homogeneity within large grains and between different grains of the same mineral. Sample CB15-19 is texturally well equilibrated compared to the other samples analysed in the study. In addition, compositional equilibrium is suggested by the preservation of eclogite-facies minerals as inclusions in garnet and the lack of zoning between these inclusions and the adjacent garnet, such as Mn-enriched rims.

While the applied Fe^{2+}-Mg thermometers differ in detail, all are subject to similar uncertainties. Any thermometer based on Fe^{2+}-Mg exchange is sensitive to Fe^{3+}/Fe^{2+}, which cannot be measured using EMP analysis. Consequently, most Fe^{2+}-Mg exchange thermometers assume no Fe^{3+} is present, thus introducing a strong bias in temperature (Powell & Holland, 2008). Although Fe^{3+}/Fe^{2+} can be calculated stoichiometrically, these calculations are also subject to their own uncertainties, and small analytical errors (e,g., in Si content) can result in large errors in final T estimates (Figure 4.1) (Ravna, 2000; Powell & Holland, 2008). Uncertainties can also result from retrograde cation exchange between minerals that were once at

equilibrium, yielding T estimates that are too low. As discussed in Chapters 5 and 6, this is an issue in the Nordøyane samples.

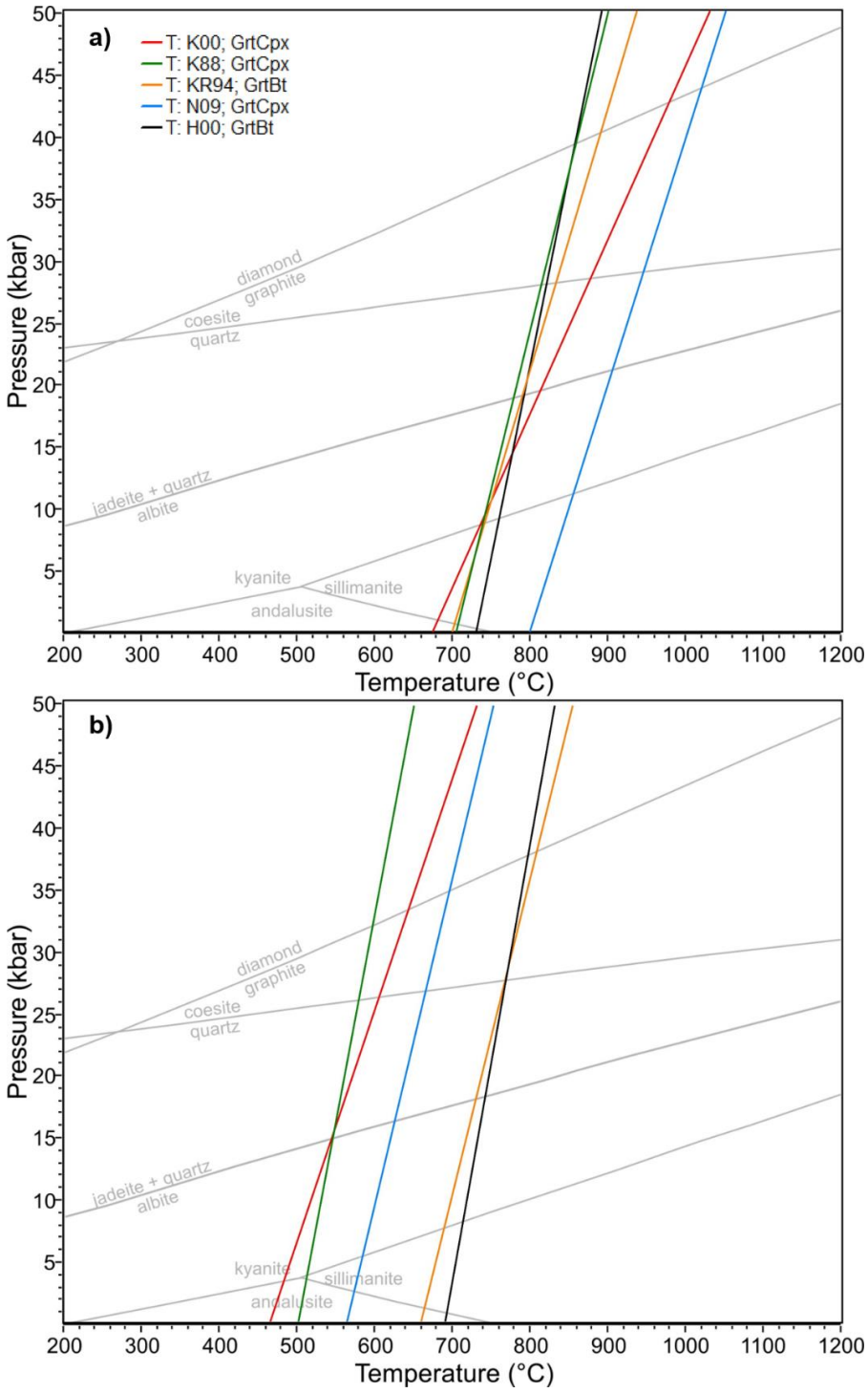

Figure 4.1. P-T outputs (PTQuick) from garnet-biotite and garnet-clinopyroxene thermometers for CB15-19 a) showing P-T estimates when using Fe^{2+} b) using Fe^{3+}. T calculated with Fe^{3+} is ca. 50-250 °C lower than T with Fe^{2+}_{total}. Chapter 5 and 6 discuss this discrepancy. (Ravna, 2000 (K00); Ravna, 1988 (K88); Kleeman and Reinhardt, 1994 (KR94); Nakamura, 2009 (N09); Holdaway, 2000 (H00))

Calculations for several conventional thermobarometers were done using the software PTQuick (Dolivo-Dobrovolsky, 2019) which allows rapid calculation of P and T for multiple combinations of data from the analysed samples. The results can be used to screen for potential problems such as disequilibrium, Fe^{3+}/Fe^{2+} (e.g., Fig. 4.1), and inconsistencies among different calibrations for the same data, allowing the user to focus on the data giving the most reliable P-T estimates.

4.4 Trace-element Thermobarometry

4.4.1 Basic Principles

A variation on conventional thermobarometery involves measuring concentrations of minor and trace elements in accessory minerals (Watson et al., 2006). The largest source of uncertainty when using trace-element thermometry is the uncertainty in the measured composition and the presence of the full assemblage used for calibration purposes. For this study, EMP was used to measure mineral compositions. The Zr-in-rutile thermometer (Tomkins et al., 2007) was used to calculate T in rutile + zircon -bearing samples. Since the Nordøyane samples contain biotite as part of the peak mineral assemblage, the Ti-in-biotite thermometer (Wu and Chen, 2015) was also used.

4.4.2 Zr-in-Rutile Thermometry

The behaviour of HFS (high field strength) elements, such as Zr, in rutile was first studied by Zack et al. (2002b). This study showed that in zircon-buffered assemblages, in medium-T eclogites and high-T granulites, the solubility of ZrO_2 in rutile is T-dependent (Zack et al. 2002, 2004). Zack et al. (2004) presented a T-dependent thermometer:

$$T(℃) = 127.8 \times \ln(\text{Zr in ppm}) - 10 \qquad \text{(eq. 4.5)}$$

(reported uncertainty of ± 50°C), calibrated by examining rutile-quartz-zircon assemblages in 31 metamorphic rocks ranging in T from 430-1100°C, with Zr concentrations in rutile between 30-8400 ppm. The study concluded that the $Zr^{4+} \leftrightarrow Ti^{4+}$ exchange in rutile is not P-dependent (Zack et al. 2004). However, Tomkins et al. (2007) predicted that the substitution of Zr^{4+} for Ti^{4+} is T- and P-dependent and that Zr in rutile should decrease with increasing P.

Tomkins et al. (2007) used experimental data to produce a calibrated rutile thermometer that consists of three calibrations, linearized in the P-T range of the α-quartz field, β-quartz field, and the coesite field. The α-quartz field follows:

$$T(℃) = \frac{83.9 + 0.410P}{0.1428 - R\ln\varphi} - 273 \quad \text{(eq. 4.6)}$$

and the coesite field:

$$T(℃) = \frac{88.1 + 0.206P}{0.1412 - R\ln\varphi} - 273 \quad \text{(eq. 4.7)}$$

where φ is Zr in ppm, P is in kbar, and R is the gas constant, 0.0083144 kJ K^{-1}. The reported uncertainty is $\pm$ 50.0 ℃ (Tomkins et al. 2007). The coesite and α-quartz field calibrations were applied to the Nordøyane eclogites.

To use this calibration to calculate T, a mineral assemblage including quartz or coesite and zircon must be present. If the rutile is not properly buffered by zircon and SiO_2 (Tomkins et al., 2007), Zr contents in rutile will be greater than predicted by eq. 4.6 resulting in an upwardly biased T estimate. This raises concern as the Nordøyane eclogites analyzed contain very rare quartz. Because inclusions of zircon and rutile are separated by the host garnet, Zr in zircon may not exchange with Ti in rutile, resulting in lower Zr contents in rutile and lower T estimates (Tomkins et al., 2007). When choosing rutile grains to analyze with the EMP, only inclusions in garnet were selected, as to minimize retrograde re-equilibration (Tomkins et al. 2007). Inclusions chosen for analysis were greater than 10 microns across as to limit any interference from the host mineral.

4.5 Thermodynamic Modelling

As an additional constraint on P-T estimates for the Nordøyane eclogites, the thermodynamic modelling program Theriak-Domino was used to produce an equilibrium phase diagram for sample CB15-19. Equilibrium phase diagrams, also called pseudo-sections, are used to predict the stable metamorphic phase assemblage in a rock with a specified bulk composition over a selected P and T range (Powell and Holland, 2008) This method is independent from conventional thermobarometry (Yakymchuk, 2017), because it is a forward-modelling approach that predicts equilibrium assemblages, whereas conventional thermobarometry is a reverse-modelling approach in which measured compositions from EMP analyses, assumed to be in equilibrium, are used to calculate P and T (Lanari and Duesterhoeft, 2019).

Theriak-Domino software (de Capitani and Petrakakis, 2010) is based on a Gibbs free energy minimization approach, using standard state thermodynamic properties, such as enthalpy

of formation and heat capacity, which have been previously determined through experimental methods and combined into internally consistent databases (Berman, 1988; Powell and Holland, 1998; Lanari and Duesterhoeft, 2019). These databases contain thermodynamic properties that are compatible with basic thermodynamic definitions, are set to one reference value, consider all the experimental data at the same time, and are able to reproduce experimental data within uncertainty (Lanari and Duesterhoeft, 2019). The JUN92 database (Berman, 1988; Aranovich and Berman, 1996) and the Holland and Powell (1998) TC55 database were used to produce the phase diagram, and were contrasted to assess reliability and consistency with thermobarometry and petrographic analyses.

Theriak-Domino calculates an equilibrium phase diagram for a specified bulk composition based on iterative calculations of mineral assemblage stabilities in a specified region of P-T space (de Capitani and Petrakakis, 2010). The program can also be used to calculate modal proportions and isopleths of specific compositional components in the predicted phase assemblage, which can be compared with observations to narrow down the P-T range in which a sample might have equilibrated. A major constraint when using this method is in assessing the reactive bulk composition at the time of peak metamorphism (Yakymchuk, 2017). The effective bulk composition of the rock can change with changes in P-T conditions and the partitioning of cations into a mineral during growth (e.g. garnet porphyroblasts) can result in zoned minerals in which the core composition may not be in equilibrium with the rest of the mineral or with the surrounding phases (Yakymchuk, 2017).

Sample CB15-19 was chosen for Theriak-Domino modelling because it is texturally homogeneous and garnet and other peak phases are compositionally homogeneous, suggesting that the sample is well equilibrated. The sample was pulverised using a jaw crusher and WC ball mill at Saint Mary's University, and the powder sent to Bureau Veritas Minerals in Vancouver for major and trace element analysis by ICP-MS (inductively coupled plasma - mass spectrometry). Nominal analytical uncertainties are ± 1% for major elements and ± 5 % for trace elements. Analytical data are reported in Appendix C.

Chapter 5: Results

5. 1 Introduction

Compositions selected for use in thermobarometers are from spatially associated and texturally well equilibrated grains. Where multiple analyses from suitable grains were available, the following criteria were used to improve the chance of recovering peak P-T conditions: maximum Na in clinopyroxene, maximum Ti in biotite, and maximum Mg in orthopyroxene. In addition, P-T conditions were calculated from average mineral compositions for each analysed domain, based on the assumption that phases in a chemically equilibrated system should have homogeneous compositions. Table 5.1 lists the important mineral formulas and abbreviations. Mineral compositions for analyses used with thermobarometers are presented in Tables 5.2-5.6, and a summary of P-T results for each sample are presented in Tables 5.7-5.9.

Table 5.1. Abbreviations, formulas, and endmembers of important minerals.

Mineral	Formula	Endmembers
Biotite (Bt)	$K_2(Fe^{2+},Mg)_6[Si_6Al_2O_{20}](OH)_4$	Annite (Ann), Phlogopite (Phl)
Garnet (Grt)	$(Mg,Fe^{2+},Mn,Ca)_3Al_2Si_3O_{12}$	Pyrope (Prp), Almandine (Alm), Spessartine (Sps), Grossular (Grs)
Omphacite (Omp)	$(Ca,Na)(Mg,Fe^{2+},Al, Fe^{3+})Si_2O_6$	Diopside (Di), Jadeite (Jd), Aegerine (Ae)
Orthopyroxene (Opx)	$(Mg,Fe^{2+})SiO_3$	Enstatite (Ens), Ferrosilite (Fs)
Rutile (Rt)	TiO_2	

5.2 Mineral Chemistry

5.2.1 Garnet

Garnet core compositions in CB15-19 range from $Prp_{41}Alm_{47}Grs_{11}Sps_{0.7}$ to $Prp_{46}Alm_{48}Grs_{10}Sps_{1,}$ averaging $Prp_{44}Alm_{46}Grs_8Sps_{0.8}$ (Figure 5.1a). The cores are homogenous (Figure 5.2), although some grains show weak but patchy Ca zoning. Garnet rims range in composition from $Prp_{40}Alm_{49}Grs_{10}Sps_{0.8}$ to $Prp_{43}Alm_{46}Grs_9Sps_{0.9}$, averaging $Prp_{42}Alm_{48}Grs_{10}Sps_9$, and are slightly enriched in Fe (Alm_{49}) compared to the core (Alm_{47}). Mn is enriched in the rims ($Sps_{0.8}$-Sps_1), which is interpreted to reflect retrogression. End-members calculated using Fe^{2+}/Fe^{3+} values for core and rim compositions of all samples are presented in Table 5.2.

In CB15-70, garnet cores vary slightly from $Prp_{46}Alm_{45}Grs_8Sps_{0.9}$ to $Prp_{47}Alm_{46}Grs_7Sps_{0.9}$. The rim compositions show a larger variation from $Prp_{40}Alm_{49}Grs_9Sps_1$ to

$Prp_{46}Alm_{46}Grs_{8}Sps_{0.9}$ (Figure 5.3). The Fe content slightly increases from Alm_{44}-Alm_{46} in the core and from Alm_{46}-Alm_{50} towards the rims where garnet is locally associated with matrix biotite. Mn and Ca remain constant across grains and there is a small variation in the Mg content through the cores, Prp_{44}-Prp_{45}. However, the Mg content decreases where garnet is adjacent to matrix amphibole and biotite from Prp_{45}-Prp_{40}.

Garnet in CB15-44 is very coarse and the compositional variation in each grain is greater than in other samples. Cores range from $Prp_{23}Alm_{40}Grs_{36}Sps_{0.4}$ to $Prp_{24}Alm_{42}Grs_{33}Sps_{0.4}$ averaging $Prp_{24}Alm_{41}Grs_{35}Sps_{0.4}$, while rims vary from $Prp_{22}Alm_{44}Grs_{34}Sps_{0.5}$ to $Prp_{24}Alm_{44}Grs_{35}Sps_{0.4}$ averaging $Prp_{23}Alm_{42}Grs_{35}Sps_{0.5}$. Garnet in this sample is much more calcic and the Ca content decreases from core to rim (Grs_{36}-Grs_{33}), as does the Fe content (Alm_{44}-Alm_{40}). Mn remains constant across the garnet grains ($Sps_{0.4}$) and is lower than in samples CB15-70 and CB15-19.

5.2.2 Omphacite

In sample CB15-19, omphacite is present as equigranular grains adjacent to garnet as well as inclusions in garnet (Figure 5.4). End-member compositions are very sensitive to Fe^{2+}/Fe^{3+}, and Fe^{3+} calculated from stoichiometry represents a maximum value. Values quoted below are based on Fe^{3+} calculations; end-member compositions using Fe^{2+} for omphacite used in thermobarometric calculations are presented in Table 5.3 and in parentheses. Omphacite inclusions in garnet vary from $Di_{62}Jd_{25}Aeg_{13}$ to $Di_{64}Jd_{21}Aeg_{15}$ ($Di_{62}Jd_{38}$ to $Di_{63}Jd_{35}$). Omphacite grains adjacent to garnet have similar compositions to the inclusions in garnet and are homogeneous.

Omphacite in CB15-70 has a similar Fe content compared to omphacite in CB15-19, however, it has a much lower Ca content and a greater Na content (Figure 5.1b). Inclusions within garnet (Figure 5.5) range from $Di_{52}Jd_{32}Aeg_{16}$ to $Di_{54}Jd_{36}Aeg_{10}$ ($Di_{52}Jd_{48}$ to $Di_{54}Jd_{46}$) and the average compositions is $Di_{53}Jd_{34}Aeg_{13}$. Like CB15-19, the large omphacites adjacent to garnets have a comparable composition to the omphacite inclusions in garnets.

In sample CB15-44, the compositions of omphacite inclusions in garnet and the omphacites adjacent to garnets differ substantially. The inclusion composition ranges from $Di_{55}Jd_{37}Aeg_{7}$ to $Di_{57}Jd_{37}Aeg_{6}$ ($Di_{55}Jd_{44}$ to $Di_{57}Jd_{43}$), showing a decrease in Fe content compared to the previously described compositions, although it has a similar overall composition to sample

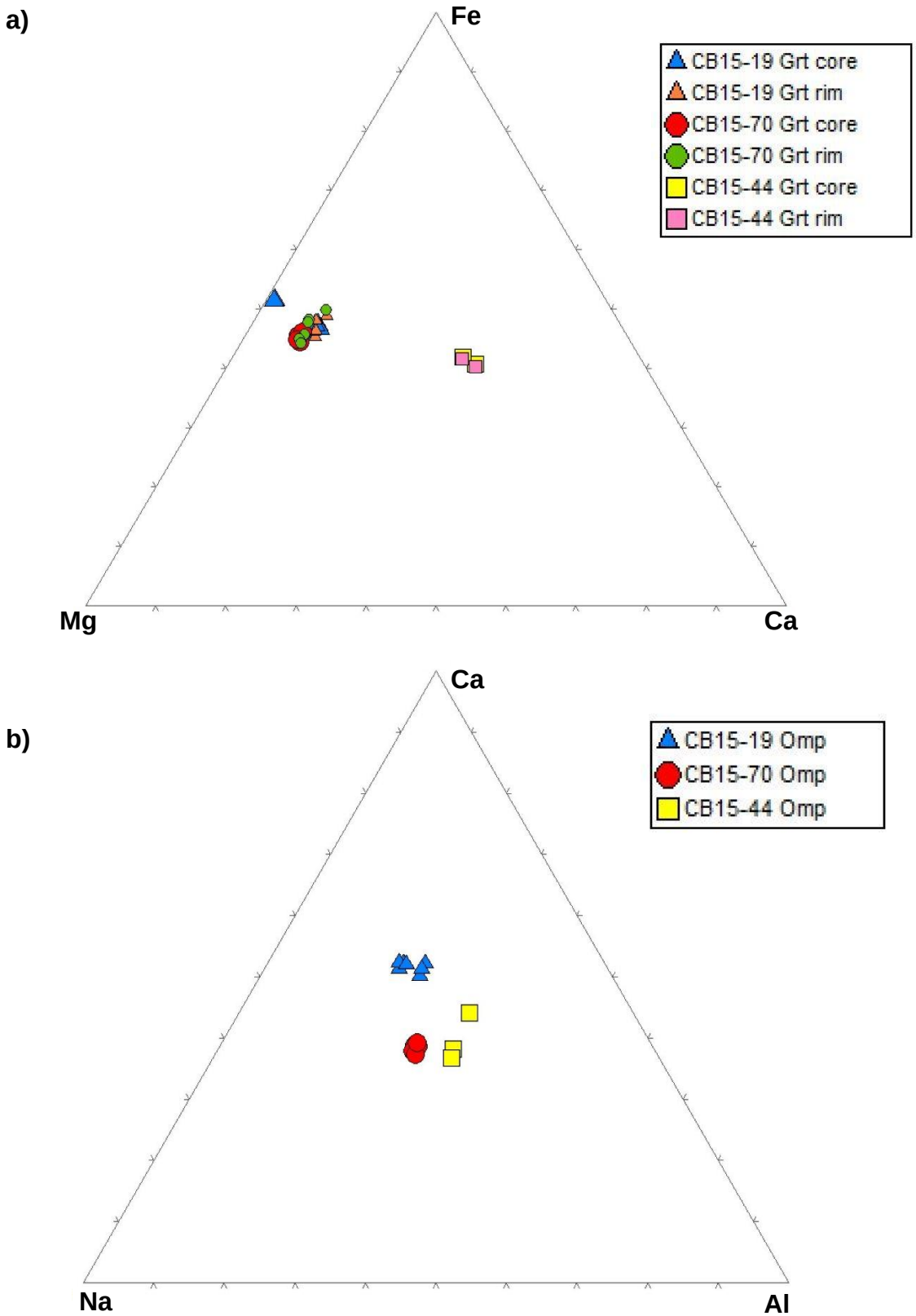

Figure 5.1. Compositional plots comparing EMP analyses used in thermobarometry a) garnet, Fe, Mg, Ca and b) omphacite, Ca, Na, Al.

CB15-70. Omphacites that are adjacent to garnet have a much higher Ca content and lower Na and Fe contents than the inclusion in garnet, $Di_{65}Jd_{30}Aeg_4$ and $Di_{67}Jd_{23}Aeg_9$ ($Di_{65}Jd_{34}$ to $Di_{67}Jd_{32}$).

5.2.3 Biotite

Biotite is present as idioblastic inclusions in garnet and as a matrix phase in CB15-19 (Figure 5.3). The compositions of biotite inclusions vary from $Ann_{26}Phl_{65}$ to $Ann_{18}Phl_{76}$. The Ti per formula unit ranges from 0.122 to as high as 0.333 (Table 5.4). Biotite inclusions in garnet in sample CB15-70 have a similar composition to those in CB15-19 ($Ann_{19}Phl_{75}$) as well as a similar Ti pfu of 0.144.

5.2.4 Orthopyroxene

Inclusions of orthopyroxene in garnet are present in samples CB15-19 and CB15-70 (Figure 5.3. The compositions presented here are based on Fe^{3+} calculations; endmembers calculated from Fe^{2+} are presented in Table 5.5. In sample CB15-19, orthopyroxene composition varies from $En_{75}Fs_{24}Wo_{0.5}$ to $En_{78}Fs_{22}Wo_{0.7}$, comparable to orthopyroxene compositions in CB15-70, which range from $En_{74}Fs_{25}Wo_{0.5}$ to $En_{76}Fs_{24}Wo_{0.3}$.

5.2.5 Rutile

Rutile inclusions in garnet are present in all the samples and are very abundant in CB15-44 (Figure 5.6). In CB15-19, the Zr content in rutile inclusions ranges from 520 ppm to 1487 ppm (Table 5.6), averaging 912 ppm. The Zr ppm of rutile in CB15-70 and in CB15-44 is like that in CB15-19. CB15-70 rutile Zr contents range from 308 to 1411 ppm, averaging 1148 ppm, while CB15-44 ranges from 419-1533 ppm.

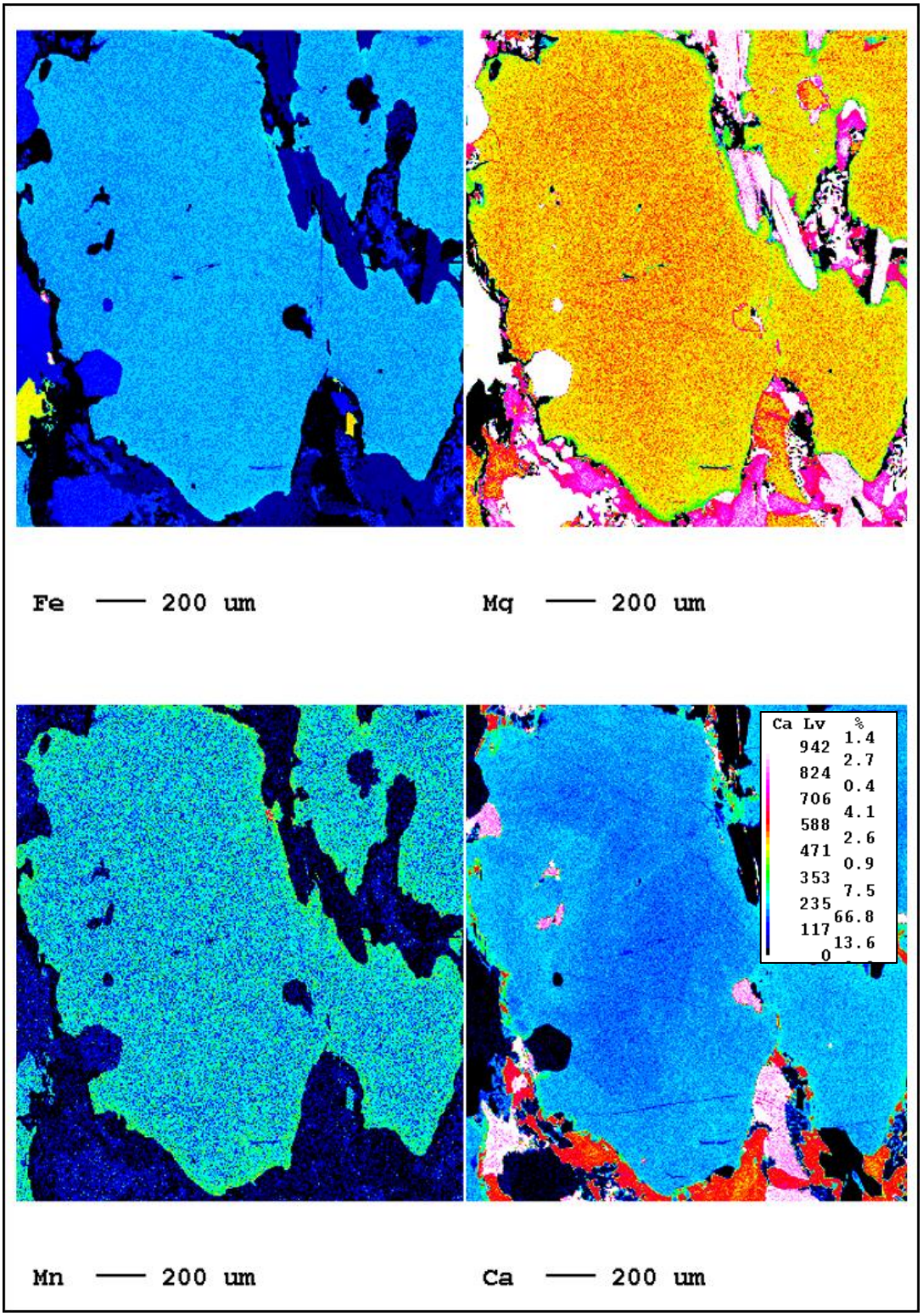

Figure 5.2. Chemical maps of the same garnet grain from Figure 5.1 showing the distribution Fe, Mg, Mn, and Ca from core to rim. Garnet in CB15-19 is homogeneous, aside from some patchy Ca zoning as shown.

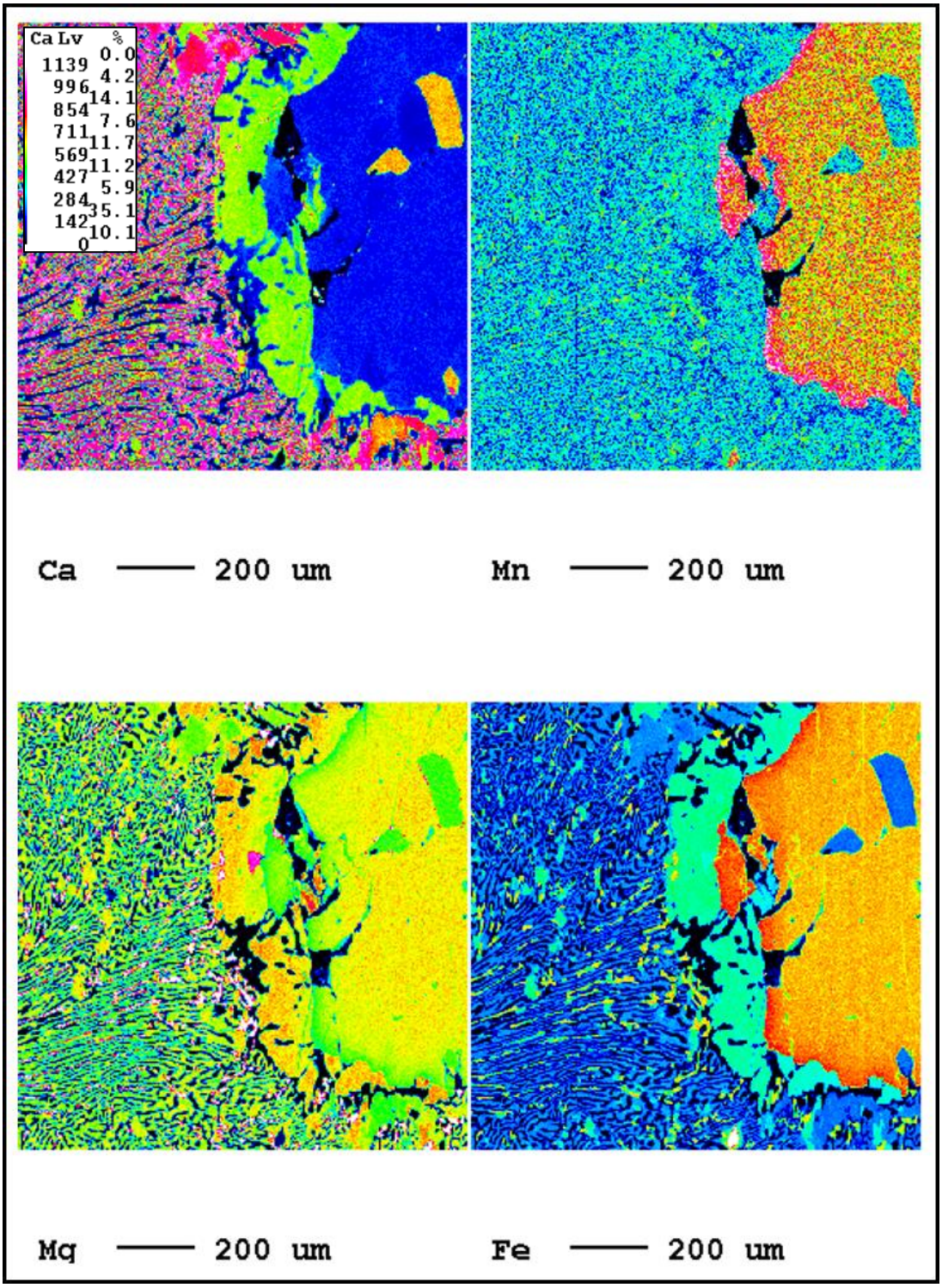

Figure 5.3. Chemical maps of garnet in sample CB15-70 showing the distribution Fe, Mg, Mn, and Ca at the rim. Adjacent to the garnet is the symplectite texture. See Figure 5.5 for more detail on the minerals present.

Table 5.2. EMP analyses of garnet rims and core averages in samples CB15-19, CB15-70, and CB15-44 used in PT calculations.

Sample		**CB15-19**			**CB15-70**			**CB15-44**
Analysis #	182	237	296-301	346	365	380, 83-4	515	520
Location	core	rim	core ave	core	rim	core ave	core	core
wt% oxides								
SiO_2	39.48	39.48	40.12	39.97	39.52	39.47	39.16	39.34
Al_2O_3	22.27	22.88	22.75	22.63	22.37	22.58	22.18	21.96
FeO	23.36	23.19	23.34	21.90	23.29	21.54	19.40	20.06
MnO	0.40	0.45	0.39	0.43	0.58	0.44	0.18	0.19
MgO	11.99	11.52	11.82	12.41	10.69	12.37	6.38	6.38
CaO	3.14	3.56	3.19	2.66	3.39	2.90	12.88	12.37
Sum	100.63	101.08	101.61	100.00	99.83	99.30	100.19	100.30
Cations pfu (based on 12 oxygens)								
Si	2.970	2.983	2.983	2.998	2.999	2.980	2.986	2.999
Al	1.975	1.992	1.993	2.000	2.000	2.010	1.993	1.973
Fe^{2+}_{tot}	1.469	1.438	1.451	1.374	1.478	1.360	1.237	1.279
Mn	0.025	0.025	0.024	0.027	0.037	0.028	0.012	0.012
Mg	1.345	1.276	1.310	1.388	1.209	1.393	0.726	0.725
Ca	0.253	0.302	0.254	0.214	0.276	0.235	1.053	1.011
Sum	8.038	8.015	8.015	8.001	7.998	8.006	8.007	7.999
mole fractions (Fe^{2+} = Fe total)								
X_{Alm}	0.475	0.476	0.477	0.454	0.493	0.451	0.409	0.423
X_{Prp}	0.435	0.421	0.431	0.462	0.403	0.462	0.240	0.240
X_{Grs}	0.079	0.094	0.084	0.076	0.092	0.078	0.348	0.334
X_{Sps}	0.008	0.009	0.008	0.009	0.012	0.009	0.004	0.004
Fe^{3+} calculated from stoichiometry (assuming sum cations = 8.000)								
Fe^{2+}	1.341	1.354	1.393	1.354	1.477	1.324	1.198	1.254
Fe^{3+}	0.122	0.093	0.055	0.008	0.001	0.035	0.037	0.024
mole fractions (Fe^{2+}/Fe^{3+} calculated)								
X_{Alm}	0.452	0.458	0.467	0.453	0.493	0.444	0.401	0.418
X_{Prp}	0.454	0.435	0.439	0.463	0.403	0.468	0.243	0.242
X_{Grs}	0.085	0.097	0.085	0.076	0.092	0.079	0.352	0.337
X_{Sps}	0.009	0.010	0.008	0.009	0.012	0.010	0.0041	0.004

$X_{Alm} = Fe/(Fe + Mg + Ca + Mn)$
$X_{Pyr} = Mg/(Fe + Mg + Ca + Mn)$
$X_{Grs} = Ca/(Fe + Mg + Ca + Mn)$
$X_{Sps} = Mn/(Fe + Mg + Ca + Mn)$

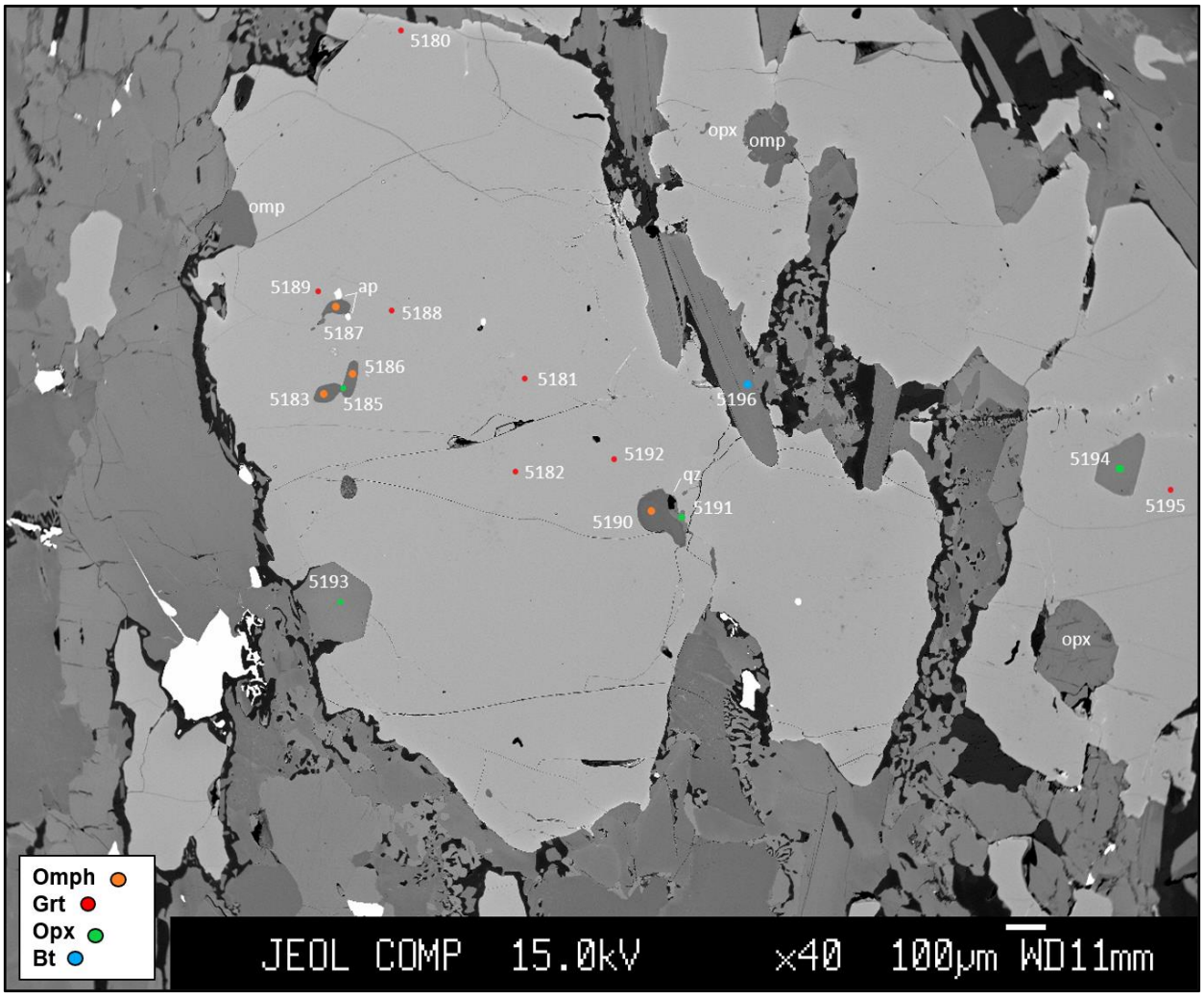

Figure 5.4. BSE image of CB15-19 showing inclusions of omphacite and orthopyroxene in garnet, as well as adjacent, matrix biotite. The 5 from each analysis displayed in Table 5.2-5.9 is dropped.

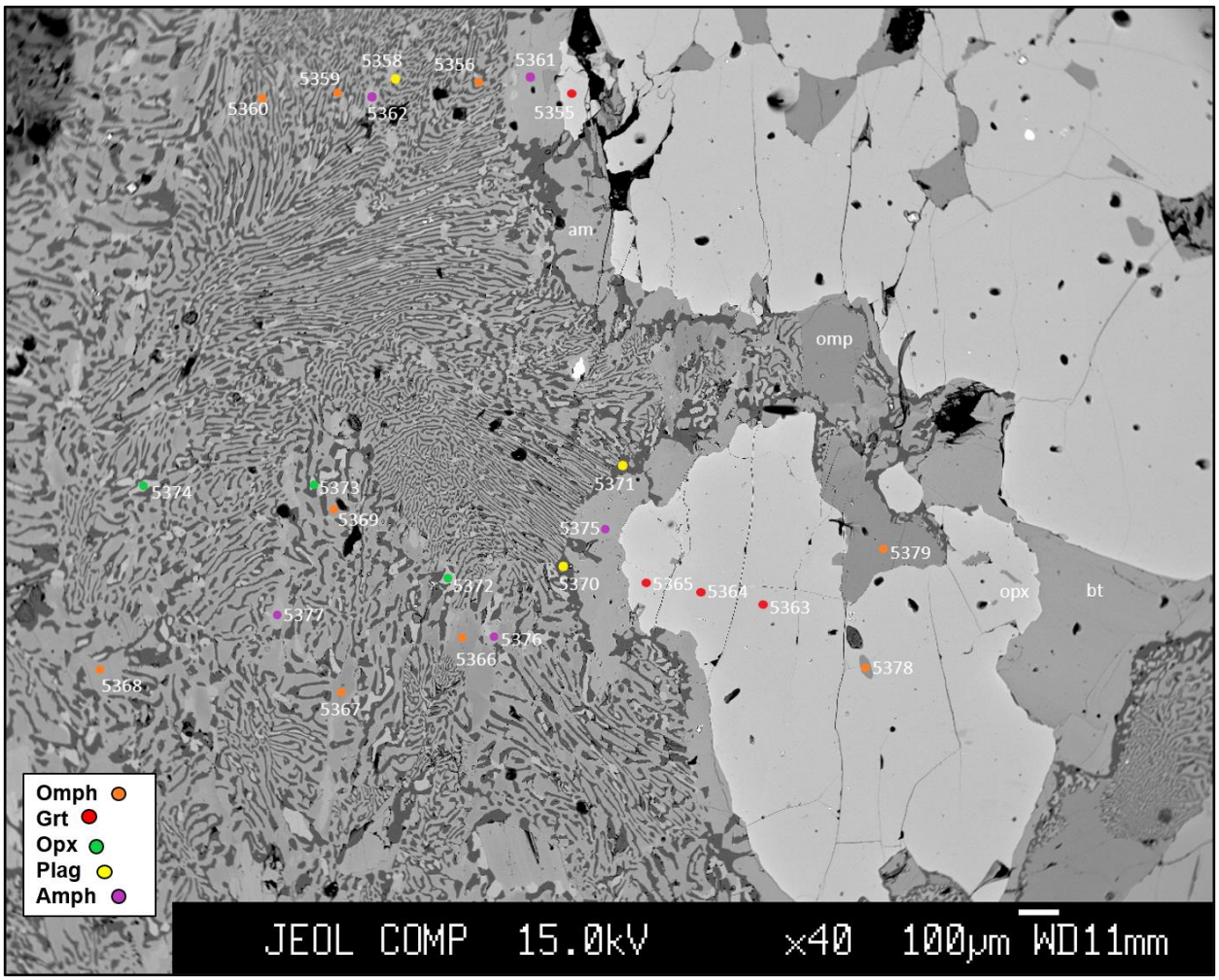

Figure 5.5. BSE image of CB15-70 showing inclusions of omphacite in garnet, as well as the well developed symplectite texture defined by plagioclase, orthopyroxene, and omphacite.

Table 5.3. EMP analyses of high and low Na omphacite inclusions and inclusions averages in garnet in samples CB15-19, CB15-70, and CB15-40 used in PT calculations.

Sample		**CB15-19**			**CB15-70**	**CB15-44**
Analysis #	187	711	268	354	533	515
Location	high Na inc	low Na inc	matrix	high Na inc	low Na inc	core ave
wt% oxides						
SiO_2	54.68	53.18	55.43	55.62	55.01	54.44
TiO_2	0.16	0.16	0.18	0.21	0.25	0.18
Al_2O_3	6.72	6.75	5.72	8.64	7.69	11.96
FeO	6.93	6.87	7.43	6.81	6.77	4.83
MgO	11.22	11.18	11.36	9.42	10.22	8.29
CaO	15.95	15.89	16.27	13.01	14.27	14.65
Na_2O	4.77	4.49	4.67	6.50	5.61	6.27
Sum	100.43	98.52	101.06	100.20	99.81	100.62
Cations pfu (based on 6 oxygens)						
Si	1.960	1.943	1.979	1.981	1.975	1.928
Ti	0.004	0.004	0.005	0.006	0.007	0.005
Al	0.284	0.291	0.241	0.362	0.325	0.499
Fe^{2+}_{tot}	0.208	0.210	0.222	0.203	0.203	0.143
Mg	0.600	0.609	0.605	0.500	0.547	0.438
Ca	0.613	0.622	0.622	0.497	0.549	0.556
Na	0.332	0.318	0.323	0.449	0.390	0.430
Sum	4.000	3.996	3.997	3.997	3.995	4.000
mole fractions (Fe^{2+} = Fe total)						
X_{Jd}	0.352	0.338	0.342	0.475	0.415	0.436
X_{Di}	0.649	0.662	0.658	0.525	0.584	0.564
Fe^{3+} calculated from stoichiometry (assuming cations = 4.000)						
Fe^{2+}	0.086	0.076	0.106	0.089	0.101	0.078
Fe^{3+}	0.121	0.134	0.116	0.114	0.102	0.065
mole fractions (Fe^{2+}/Fe^{3+} calculated)						
X_{Jd}	0.223	0.196	0.220	0.355	0.307	0.370
X_{Di}	0.649	0.662	0.658	0.525	0.584	0.564
X_{Ae}	0.129	0.142	0.122	0.120	0.108	0.066

$X_{Jd} = (Na - Fe^{3+})/(Fe^{3+} + (Na - Fe^{3+}) + Ca)$

$X_{Di} = Ca/(Fe^{3+} + (Na - Fe^{3+}) + Ca)$

$X_{Ae} = Fe^{3+}/(Fe^{3+} + (Na - Fe^{3+}) + Ca)$

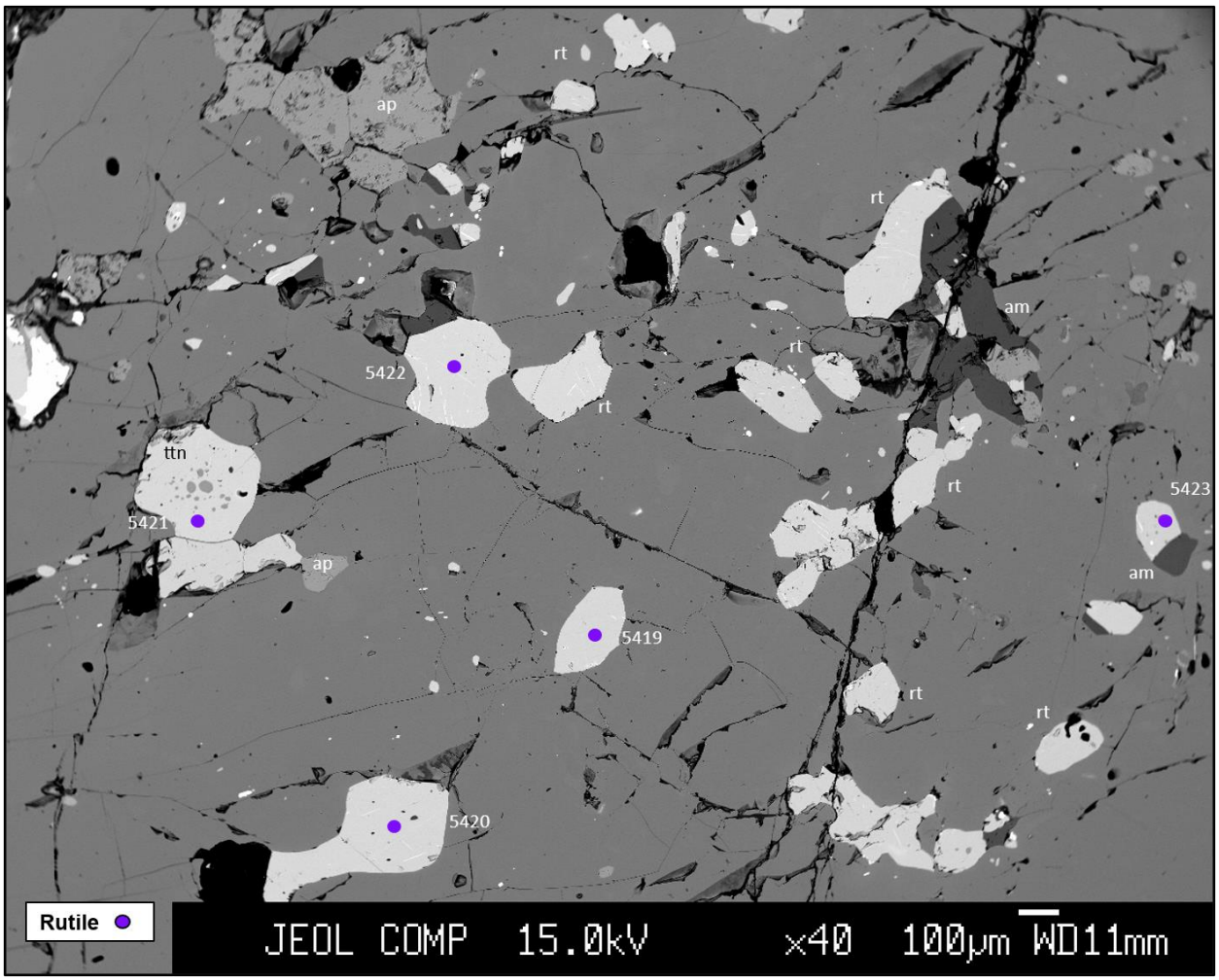

Figure 5.6. BSE image of coarse-grained garnet in sample CB15-44 with abundant rutile and titanite inclusions.

Table 5.4. EMP analyses of average biotite inclusions in garnet, high Ti inclusions, and matrix in samples CB15-19 and CB15-70.

`		CB15-19		CB15-70
Analysis #	718-20	252	234	814
Location	ave inc	matrix	high Ti	inc
wt% oxides				
SiO_2	38.99	37.81	38.66	39.89
TiO_2	2.53	3.81	6.16	2.66
Al_2O_3	13.73	15.96	14.35	13.82
FeO	8.00	10.88	10.37	8.54
MgO	20.68	17.71	17.48	20.40
Na_2O	0.37	0.52	0.62	0.57
K_2O	9.12	9.01	8.79	9.27
Cl	0.11	0.07	0.07	0.30
F	0.18	0.11	0.10	0.24
Sum	93.72	95.88	96.61	95.68
Cations pfu (based on 11 oxygens)				
Si	2.862	2.748	2.781	2.882
Ti	0.140	0.208	0.333	0.144
Al	1.188	1.368	1.217	1.177
Fe^{2+}_{tot}	0.491	0.662	0.624	0.516
Mg	2.266	1.919	1.874	2.196
Na	0.053	0.073	0.087	0.079
K	0.854	0.835	0.807	0.854
Cl	0.014	0.009	0.009	0.036
F	0.042	0.025	0.024	0.055
Sum	7.912	7.848	7.756	7.943
mole fractions (Fe^{2+} = Fe total)				
X_{Phl}	0.768	0.660	0.662	0.753
X_{Ann}	0.175	0.245	0.250	0.186
Fe^{3+} calculated from stoichiometry (assuming cations = 8.000)				
Fe^{2+}	0.433	0.601	0.565	0.464
Fe^{3+}	0.058	0.061	0.059	0.052
mole fraction (Fe^{2+}/Fe^{3+} calculated)				
X_{Phl}	0.671	0.673	0.676	0.767
X_{Ann}	0.272	0.23.2	0.236	0.172

$X_{Phl} = Mg/(Al^{VI+} + Cr + Fe + Mn + Mg + Ti)$

$X_{Ann} = Fe/(Al^{VI+} + Cr + Fe + Mn + Mg + Ti)$

Table 5.5. EMP analyses of average orthopyroxene inclusions in garnet and high Mg orthopyroxene inclusions in garnet for samples CB15-19 and CB15-70.

Sample	**CB15-19**		**CB15-70**	
Analysis #	194, 227	185	399,400	821
Location	ave inc	high Mg inc	ave inc	high Mg inc
wt% oxides				
SiO_2	54.45	53.55	53.99	56.43
Al_2O_3	1.11	0,86	1.11	0.71
FeO	17.09	17.29	16.28	15.97
MnO	0.09	0.11	0.11	0.12
MgO	27.27	27.37	27.06	28.12
CaO	0.27	0.29	0.23	0.19
Sum	100.28	99.46	98.78	101.6
Cations pfu (based on 6 oxygens)				
Si	1.960	1.939	1.969	1.997
0Al	0.047	0.076	0.048	0.029
Fe^{2+}_{tot}	0.514	0.471	0.497	0.473
Mn	0.003	0.002	0.003	0.004
Mg	1.464	1.497	1.471	1.484
Ca	0.011	0.013	0.009	0.007
Sum	3.998	3.997	3.997	3.993
mole fractions (Fe^{2+} = Fe total)				
X_{Wo}	0.005	0.006	0.005	0.004
X_{En}	0.736	0.756	0.744	0.756
X_{Fs}	0.259	0.238	0.251	0.241
Fe^{3+} calculated from stoichiometry (assuming cations = 4.000)				
Fe^{2+}	0.476	0.418	0.478	0.473
Fe^{3+}	0.038	0.053	0.018	0.000
mole fractions (Fe^{2+}/Fe^{3+} calculated)				
X_{Wo}	0.005	0.007	0.005	0.004
X_{En}	0.751	0.777	0.751	0.756
X_{Fs}	0.244	0.217	0.244	0.241

$X_{Wo} = Ca/(Ca + Mg + Fe)$
$X_{En} = Mg/(Ca + Mg + Fe)$
$X_{Fs} = Fe/(Ca + Mg + Fe)$

Table 5.6. EMP analyses of rutile inclusions in garnet for samples CB15-19, CB15-70, and CB15-44.

Sample		**CB15-19**			**CB15-70**		**CB15-44**	
Analysis #	325	237	314,17	560	559	557-558	422	423
Location	high Zr	low Zr	inc ave	high Zr	low Zr	inc ave	low Zr	high Zr
wt% oxides								
TiO_2	99.50	100.30	100.45	98.67	98.31	98.30	101.07	99.03
FeO	0.77	0.45	0.57	0.26	0.23	0.44	0.21	0.25
CaO	0.37	0.16	0.05	0.02	0.08	0.06	0.004	0.05
ZrO_2	0.15	0.05	0.09	0.14	0.03	0.11	0.04	0.15
V_2O_3	0.42	0.39	0.47	0.37	0.33	0.43	0.60	0.69
Nb_2O_5	0.94	0.23	0.33	0.51	0.32	0.12	0.07	0.04
Sum	102.15	101.59	101.97	100.00	99.29	99.45	102.00	100.22
Cations pfu (based on 2 oxygens)								
Ti	0.981	0.991	0.989	0.989	0.992	0.992	0.994	0.991
Fe^{2+}_{tot}	0.001	0.005	0.006	0.003	0.003	0.005	0.002	0.002
Ca	0.005	0.002	0.0008	0.0002	0.001	0.0009	0.000	0.0008
Zr	0.001	0.0003	0.0006	0.0009	0.0002	0.0007	0.0003	0.001
V	0.004	0.004	0.005	0.004	0.004	0.005	0.006	0.007
Nb	0.006	0.001	0.002	0.003	0.002	0.001	0.0004	0.0002
Sum	1.006	1.004	1.004	1.000	1.002	1.004	1.003	1.004
Zr in ppm	1487	520	912	1411	308	1148	419	1533

5.3 Thermobarometry

5.3.1 Approach

Several conventional thermobarometric methods were applied to samples CB15-19, 70, and 44, with the purpose of estimating peak temperature conditions (Tmax and P @ Tmax) for these samples. The Fe-Mg exchange thermometers require a P estimate in order to calculate T; in this case P of 20 and 30 kb was assumed to cover the pressure range of interest for UHP rocks. All T calculations were done for both the $Fe_{total} = Fe^{2+}$ and calculated Fe^{3+} cases; these represent maximum and minimum T, respectively. Garnet-clinopyroxene thermometry was done via Excel for the $Fe_{total} = Fe^{2+}$ case, and the T estimates for calculated Fe^{3+}/Fe^{2+} values were done with PTQuick. Garnet-biotite, Ti-in-biotite, and garnet-orthopyroxene thermometry was done using PTQuick, as this program uses the conventions proposed by the original authors.

The P-T results for sample CB15-19 are from multiple, texturally equilibrated garnet grains and inclusions hosted by garnets, as well as from rutile grains situated within garnet cores. Inclusions of orthopyroxene, omphacite, and biotite were paired with the host garnet to produce T estimates at an assumed pressure. Sample CB15-70 comprises a similar mineral assemblage and the same thermometers were used. Sample CB15-44 has experienced much more hydration than the other samples and therefore comprises more amphibole than pyroxene, and biotite is much sparser as inclusions in garnet. A description of the general approach for each thermometer follows.

5.3.1 Garnet-Clinopyroxene Thermometry

Microprobe analyses of omphacite inclusions and the adjacent host garnet were combined to obtain T estimates using the garnet-clinopyroxene thermometer from Ravna (2000). Inclusions within garnet could represent the prograde assemblage and are minerals that were present at the time the garnet grew, therefore, they are more likely to preserve peak T than matrix omphacite which has experienced some degree of retrogression. Omphacite inclusions chosen for analysis are typically idioblastic to subidioblastic, distributed closer to the core of the host garnet, and well-isolated from fractures. Compositional mapping of host garnets (e.g., Figure 5.2, 5.3) was used to assess whether omphacite inclusions and adjacent garnets were affected by retrograde zoning.

For sample CB15-19, garnet-clinopyroxene Fe^{2+}-Mg thermometry applied to coexisting garnet and omphacite (eq. 4.4) gave a T range of 801-834 ± 50 °C at 20 kb, and 872-908 ± 50 °C at 30 kb, assuming $Fe_{total} = Fe^{2+}$ (Table 5.7). The average Ts are 817 ± 50 °C and 889 ± 50 °C at 20 and 30 kb respectively. Using the highest Ca analysis in garnet and the highest Na analysis in omphacite, the T is 840 ± 50 °C at 20 kb and 914 ± 50 °C at 30 kb. For calculated Fe^{2+}/Fe^{3+} values, the T range dropped significantly to ca. 350-500 ± 50 °C at 20 kb and ca. 500-650 ± 50 °C at 30 kb.

For sample CB15-70, garnet-clinopyroxene thermometry yielded temperatures ca. 100 °C greater than CB15-19 and ranged 867-910 ± 50 °C at 20 kb, and 944-988 ± 50 °C at 30 kb, averaging 898-977 ± 50 °C at 20-30 kb, when $Fe^{2+} = Fe_{total}$. The T range decreased to 540-650 ± 50 °C at 20 kb and 590-715 ± 50 °C at 30 kb, averaging ca. 600-660 ± 50 °C for 20-30 kb, when using Fe^{2+}/Fe^{3+} (Table 5.8).

Temperatures for sample CB15-44 calculated by garnet-clinopyroxene thermometry were in between those of 19 and 70 and ranged from 858-869 ± 50 °C at 20 kb and from 887-928 ± 50 °C at 30 kb, averaging 863-922 ± 50 °C between 20-30 kb (Table 5.9). Temperatures were greater than sample 19 and 70 when calculating with Fe^{2+}/Fe^{3+} values and varied from 649-709 ± 50 °C at 20 kb and 696-759 ± 50 °C at 30 kb, with an average of 679-727 ± 50 °C for 20-30 kb.

5.3.2 Garnet-Biotite Thermometry

The majority of garnet-biotite thermometers, including the Holdaway (2000) calibration used here, have been calibrated for pelitic bulk compositions and much lower P-T ranges than the eclogite facies conditions in these rocks. Biotite is present as idioblastic inclusions in garnet in samples CB15-19 and CB15-70. Analyses were taken from biotite inclusions that are isolated from fractures in the host garnet and are distributed closer to garnet cores. Retrograde exchange strongly affects the composition of biotite, so matrix biotite analyses were not used in the thermometry calculations.

For sample CB15-19, garnet-biotite thermometry applied to biotite inclusions and host garnets produced temperatures of 700-800 ± 25 °C at 20 kb and 733-833 ± 25 °C at 30 kb, averaging 739-804 ± 25 °C for 20-30 kb ($Fe^{2+} = Fe_{total}$). Calculated Fe^{2+}/Fe^{3+} had a ± 10 °C effect on the average temperature estimate, though individual Fe^{3+} T estimates are presented in Table 5.7. Garnet-biotite thermometry applied to sample CB15-70 gave T of 744-799 ± 25 °C at 20-30 kb ($Fe^{2+} = Fe_{total}$).

5.3.3 Garnet-Orthopyroxene Thermometry

In samples CB15-19 and CB15-70, orthopyroxene is typically situated in the matrix, however, there are sparse idioblastic inclusions hosted in the cores of garnet grains. The Harley (1984) garnet-orthopyroxene calibration was used to calculate T estimates for these inclusions and adjacent host garnets using PTQuick.

Garnet-orthopyroxene for sample CB15-19 yielded lower temperatures than garnet-clinopyroxene results. Temperatures ranged from 735-748 ± 40 °C at 20 kb and from 788-803 ± 40 °C at 30 kb when using Fe^{2+}, averaging 742-795 ± 40 °C for 20-30 kb. When using Fe^{2+}/Fe^{3+}, the T results only differed by ± 3 °C (Table 5.7). For sample CB15-70, T estimates for 70 are slightly higher than those for sample 19. T ranges from 769-783 ± 40 °C at 20 kb and 825-840 ± 40 °C at 30 kb.

5.3.4 Ti-in-Biotite Thermometry

Ti-in-biotite thermometry from Wu and Chen (2015) was applied to biotite inclusions that are hosted in garnets in sample CB15-19 and CB15-70. Unlike the previously mentioned thermometers, Ti-in-biotite thermometry is unaffected by the issue of Fe^{2+}/Fe^{3+} values, and because biotite exists as inclusions in garnet, it is assumed that retrograde exchange would not alter the biotite composition. For sample CB15-19, Ti-in-biotite thermometer yielded a T range of 708-783 ± 50 °C at 20 kb and 824-910 ± 50 °C at 30 kb, averaging 733-825 ± 50 °C for 20-30 kb (Table 5.7). The T range for CB15-70 is 735-853 ± 50 °C for the same pressure range (Table 5.8).

5.3.5 Zr-in-Rutile Thermometry

The Zr-in-rutile thermometer (Tomkins et al., 2007) results presented here are from rutile inclusions hosted in adjacent garnets from samples CB15-19, 44, and 70. Unlike Fe^{2+}-Mg exchange thermometry, Zr-in-rutile thermometry is not known to be affected by retrograde cation exchange, as rutile and zircon inclusions are generally separated by garnet. The rutile inclusions analyzed were typically greater than 100 microns across to minimize interference from surrounding mineral phases (Hilchie, unpublished data), however, some inclusions were slightly less than 100 microns.

The Zr-in-rutile thermometer applied to rutile inclusions in garnet in CB15-19 gave a T range of 743-820 ± 50 °C at 20 kb using the α-quartz calibration (eq. 4.6) averaging 792 ± 50 °C,

while the coesite calibration (eq. 4.7) produced a T range of 786-868 ± 50 °C at 30 kb, averaging 838 ± 50 °C (Table 5.7). When applied to CB15-70, T results are slightly higher than CB15-19, ranging from 782-817 ± 50 °C at 20 kb (eq. 4.6) and 827-864 ± 50 °C at 30 kb (eq. 4.7) averaging 803-850 ± 50 °C for 20-30 kb (Table 5.8). For CB15-44, the thermometer yielded Ts of 695-749 ± 50 °C at 20 kb (eq. 4.6) and 735-792 ± 50 °C at 30 kb (eq. 4.7), averaging 724-765 ± 50 °C for the pressure range (Table 5.9).

Table 5.7. PT results for sample CB15-19. EMP analyses for some of these analyses presented in Tables 5.1-5.4 and appendix A. T calculated using $Fe_{total} = Fe^{2+}$, see text for detail. Values bolded and italicized use Fe^{3+}. Pressures are assumed, not calculated. Uncertainties as quoted in source papers.

Sample CB15-19 Thermobarometer	Analyses Used	T (°C) @ 20 kb	T (°C) @ 30 kb
Grt-Cpx	ave Grt 182, 192, 181, 188, 189,	815 ± 50	888 ± 50
(R00)	ave Omph 183, 186, 187, 190	***515 ± 50***	***567 ± 50***
	ave Grt 742, 743; Omph 701	814 ± 50	885 ± 50
		317 ± 50	***355 ± 50***
	ave Grt 744, 745; Omph 705	834 ± 50	908 ± 50
		464 ± 50	***513 ± 50***
	ave Grt 746, 747, 748; ave Omph 709, 710, 711	820 ± 50	892 ± 50
		463 ± 50	***511 ± 50***
	Grt 172; Omph 173	801 ± 50	872 ± 50
		516 ± 50	***568 ± 50***
Grt-Bt	ave Grt 749, 750; ave Bt 716,717	699 ± 25	733 ± 25
(H00)	ave Grt 751, 752; ave Bt 718, 719, 720	709 ± 25	758 ± 25
	Grt 206; Bt 234	760 ± 25	790 ± 25
	ave Grt 171, 172; ave Bt 165, 166, 167	726 ± 25	759 ± 25
	Grt 808; Bt 812	800 ± 25	833 ± 25
Grt-Opx	Grt 195; Opx 194	716 ± 50	832 ± 50
(H84)	ave Grt 182, 188; ave Opx 185, 193	778 ± 40	834 ± 40
	ave Grt 211, 212; ave Opx 227, 228	764 ± 40	819 ± 40
Ti-in-Bt	ave Bt 716, 717	716 ± 50	832 ± 50
(WC15)	ave Bt 718, 719, 720	726 ± 50	844 ± 50
	ave Bt 165, 166,167	731 ± 50	849 ± 50
	Bt 250	783 ± 50	910 ± 50
Zr-in-Rt	Rt 314	781 ± 50	826 ± 50
(T08)	Rt 317	743 ± 50	763 ± 50
	Rt 323	774 ± 50	819 ± 50
	Rt 327	801 ± 50	848 ± 50
	Rt 328	813 ± 50	860 ± 50
	Rt 000	820 ± 50	868 ± 50

Table 5.8. PT calculations for sample CB15-70. EMP analyses for these minerals presented in Tables 5.1-5.4 and appendix A. Nonbolded values use $Fe_{total} = Fe^{2+}$ and bolded and italicized values use Fe^{3+}. Pressure is assumed.

Sample CB15-70 Thermobarometer	Analyses Used	T (°C) @ 20 kb	T (°C) @ 30 kb
Grt-Cpx	ave Grt 346, 347, 348	907 ± 50	987 ± 50
(R00)	ave Omph 352, 353, 354	***617 ± 50***	***678 ± 50***
	ave Grt 363, 364; Omph 37	896 ± 50	975 ± 50
		539 ± 50	***648 ± 50***
	Grt 395; Omph 39	900 ± 50	979 ± 50
		523 ± 50	***587 ± 50***
	Grt 349; Omph 533	867 ± 50	944 ± 50
		595 ± 50	***654 ± 50***
	ave Grt 542, 543, 544; ave Omph 537, 538, 539	908 ± 50	988 ± 50
		594 ± 50	***652 ± 50***
Grt-Bt (H00)	Grt 816; Bt 814	744 ± 25	779 ± 25
Grt-Opx (H84)	ave Grt 390, 391; ave Opx 399, 400	783 ± 40	840 ± 40
Ti-in-Bt (WC15)	Bt 814	735 ± 50	853 ± 50
Zr-in-Rt (T08)	Rt 557	817 ± 50	864 ± 50
	Rt 558	807 ± 50	853 ± 50
	Rt 563	782 ± 50	827 ± 50

Table 5.9. PT calculations using the grt-cpx and Zr-in-rutile thermometers for sample CB15-44. EMP analyses for these minerals presented in Tables 5.1-5.4 and appendix A. Nonbolded values use $Fe_{total} = Fe^{2+}$ and bolded and italicized values use Fe^{3+}. Pressure is assumed.

Sample CB15-44 Thermobarometer	**Analyses Used**	**T (°C) @ 20 kb**	**T (°C) @ 30 kb**
Grt/Cpx (H00)	Grt 515; Omph 497	869 ± 50	928 ± 50
		709 ± 50	***759 ± 50***
	Grt 520; Omph 498	858 ± 50	916 ± 50
		649 ± 50	***696 ± 50***
Zr-in-Rt (T08)	Rt 422	695 ± 50	735 ± 50
	Rt 426	749 ± 50	792 ± 50
	Rt 427	715 ± 50	756 ± 50
	Rt 431	743 ± 50	786 ± 50
	Rt 432	715 ± 50	756 ± 50

5.4 Theriak-Domino Results

Thermodynamic modelling with Theriak-Domino was used to constrain P-T results further using the bulk composition of CB15-19. The equilibrium diagram presented here used the Thermocalc database, TC55 (Holland and Powell, 2008), and predicts an assemblage of garnet + omphacite + orthopyroxene + biotite + rutile + quartz/coesite + H_2O stable over a broad range of P-T conditions spanning the quartz-coesite boundary (Figure 5.7). The JUN92 database (Berman and Aranovich, 1996) used initially to test the method also produced a field with the same mineral assemblage stable in the vicinity of the quartz-coesite transition. However, the Thermocalc database incorporates melting, which the JUN92 database does not, and it also has a more realistic amphibole model. For these reasons, only the equilibrium diagrams from produced from the Thermocalc database are used.

The modal proportion isolines (isomodes) calculated using both databases are extremely similar, with ca. 40% garnet, 7% biotite, 18% orthopyroxene, 32% omphacite, 1% rutile, and 2% α-quartz, approximately consistent with the petrographic observations described in Chapter 3. Since there is virtually no variation across the region of interest, the isomodes do not serve to narrow down the P-T range and are not shown in the following diagrams. The mineral composition isopleths are more revealing (Figure 5.8). Of the various components plotted, XJd and XPrp yield results compatible with the observed mineral data in the correct field (Figure 5.9). The discrepancy between other model isopleths and the observations has been interpreted as a result of retrogression and is discussed further in Chapter 6.

For sample CB15-19, model isopleths overlap with measured XJd and XPrp over the P-T range 800-840 °C and ca. 24-32 kb (Figure 5.9a). When the Zr-in-rutile isopleths are added the P-T range narrows to 800-820 °C and ca. 25-32 kb (Figure 5.9b).

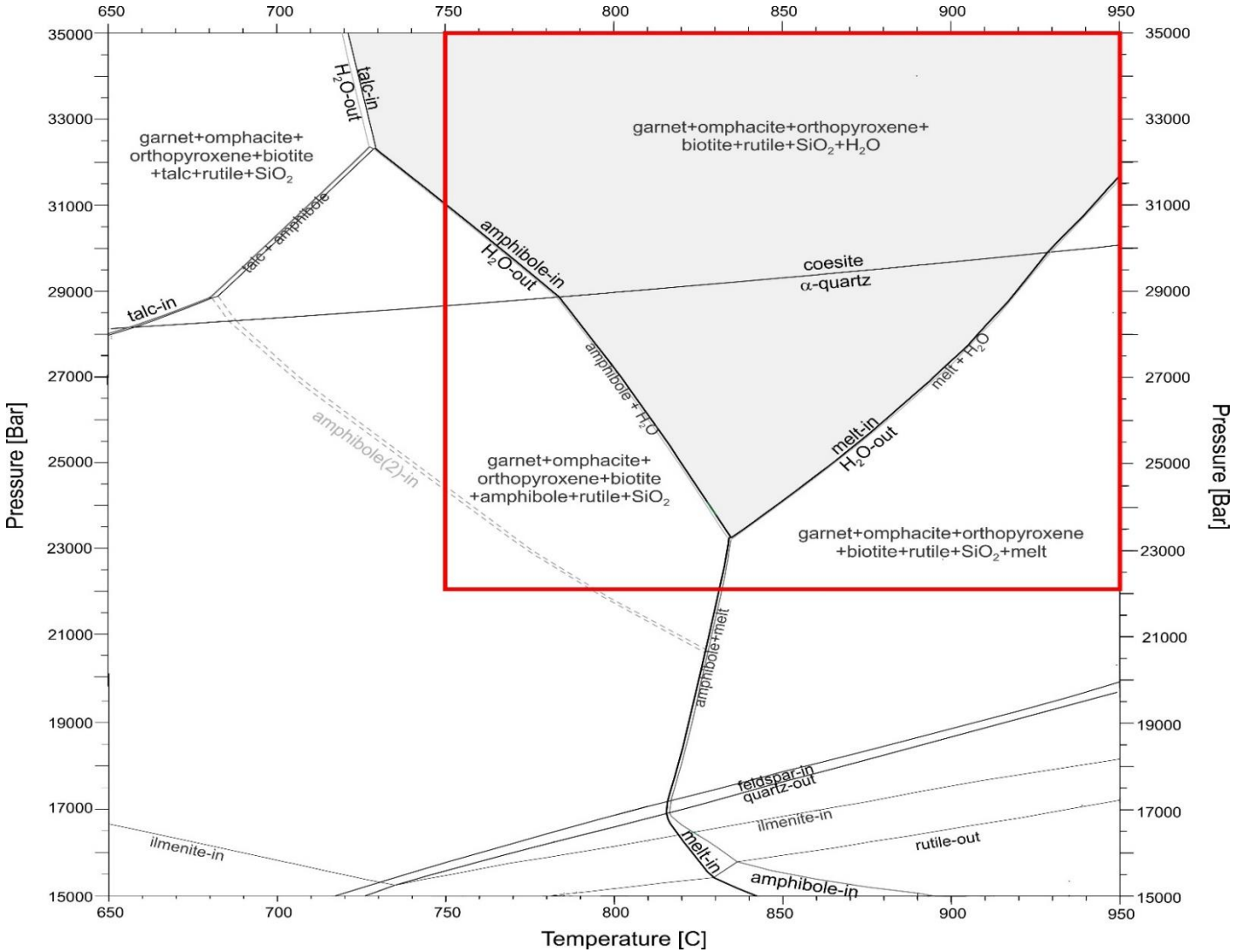

Figure 5.7. Phase equilibrium diagram produced from Theriak-Domino using the bulk composition of CB15-19 for the P-T range 650-950 °C and 15-35 kb. The grey shaded area shows the stability of the CB15-19 mineral assemblage. The red box highlights the P-T field of interest used in isopleth models (Figure 5.8 a-f)

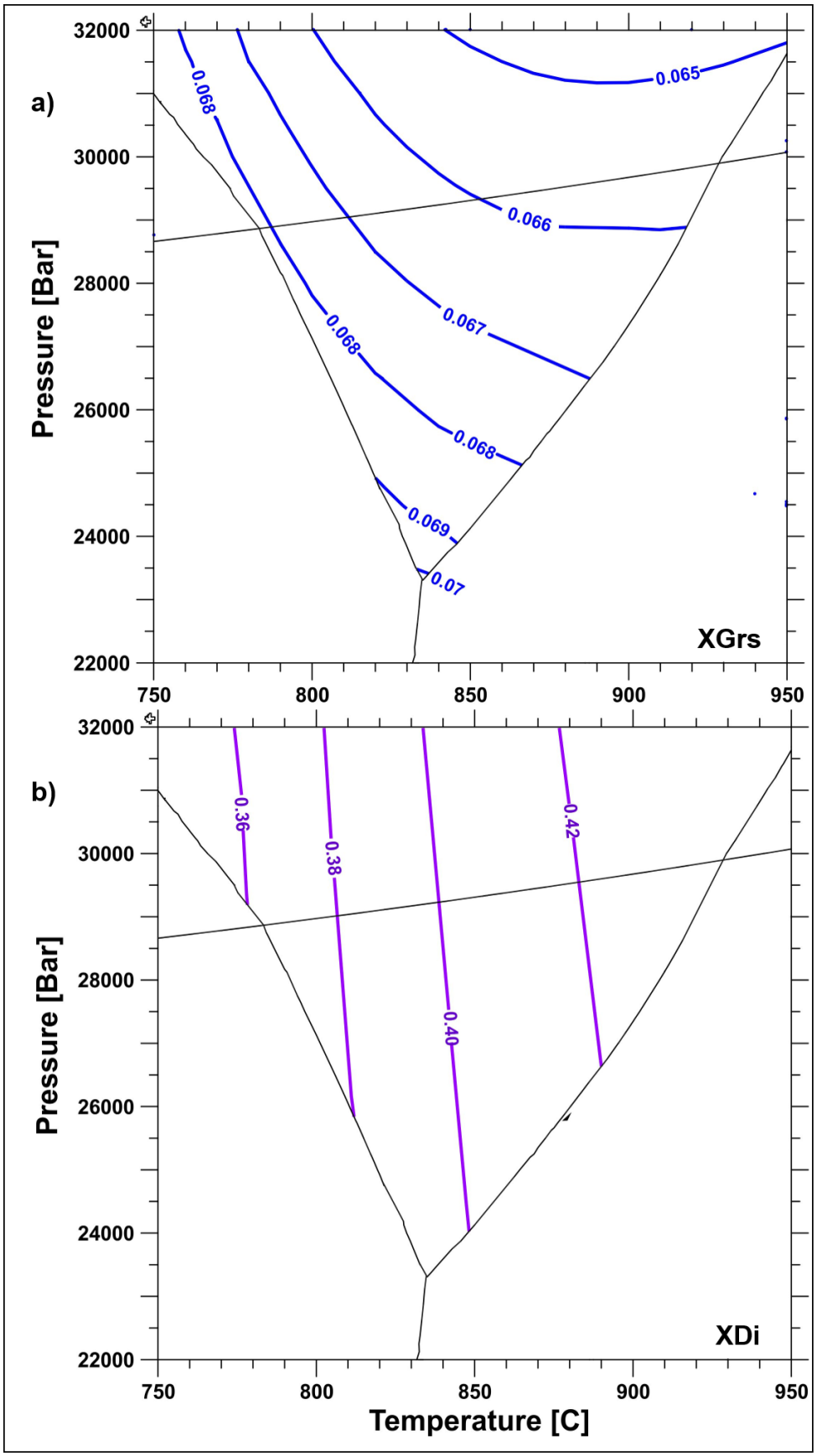
a)
Pressure [Bar]
32000
30000
28000
26000
24000
22000
750
800
850
900
950
0.065
0.066
0.067
0.068
0.068
0.068
0.069
0.07
XGrs
b)
Pressure [Bar]
0.36
0.38
0.40
0.42
XDi
Temperature [C]

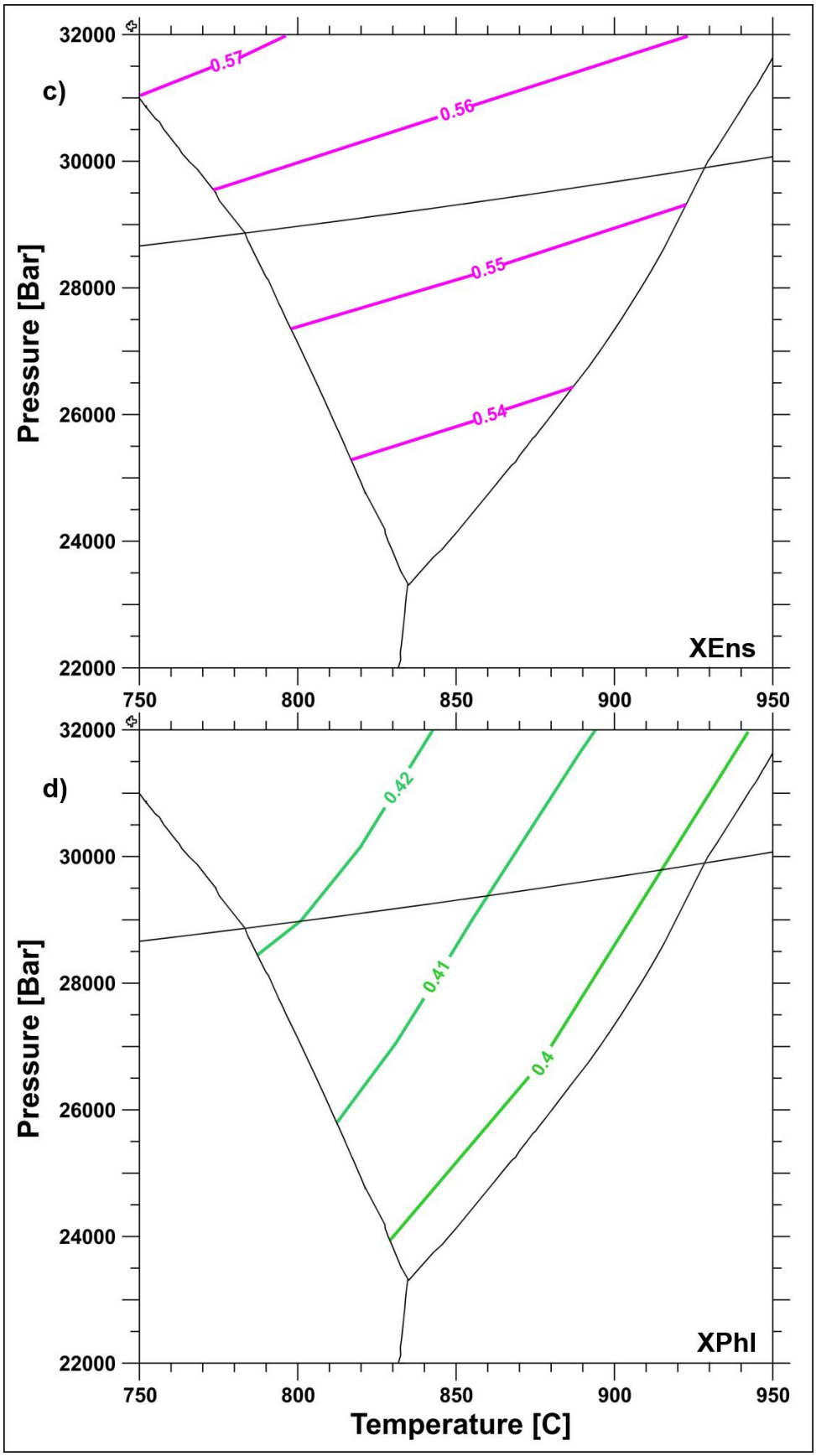
c)
0.57
0.56
0.55
0.54
XEns
d)
0.42
0.41
0.4
XPhl
Pressure [Bar]
Temperature [C]
32000
30000
28000
26000
24000
22000
750
800
850
900
950

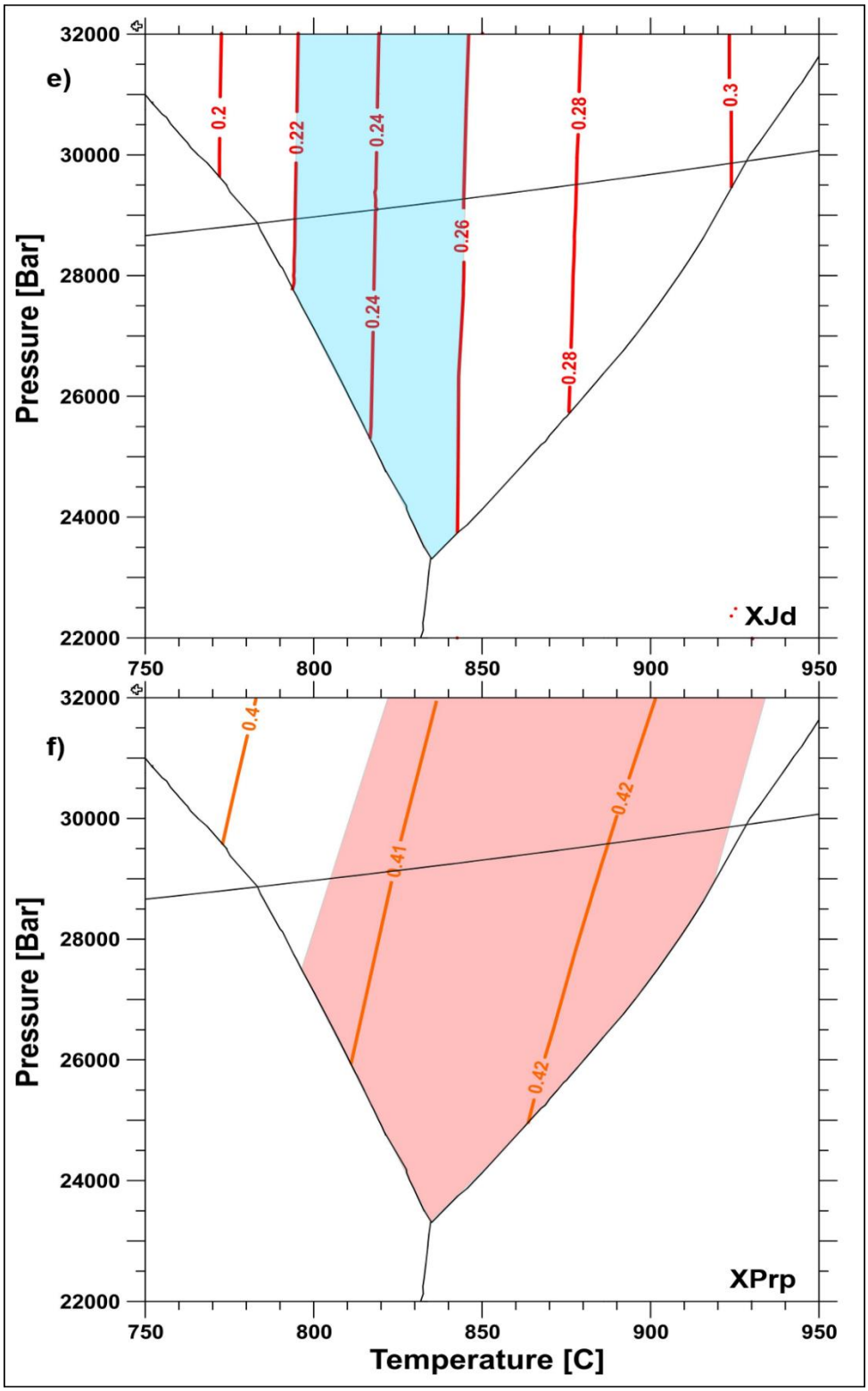

Figure 5.8. Model isopleth diagrams of a) XGrs in garnet b) XDi in omphacite c) XEns in orthopyroxene d) XPhl in biotite e) XJd in omphacite, and f) XPrp in garnet. Only the isopleths of XJd and XPrp overlap with the observed data as indicated in the shaded field. For XJd, this is between 0.22-0.26, and ca. 0.408-0.425 for XPrp.

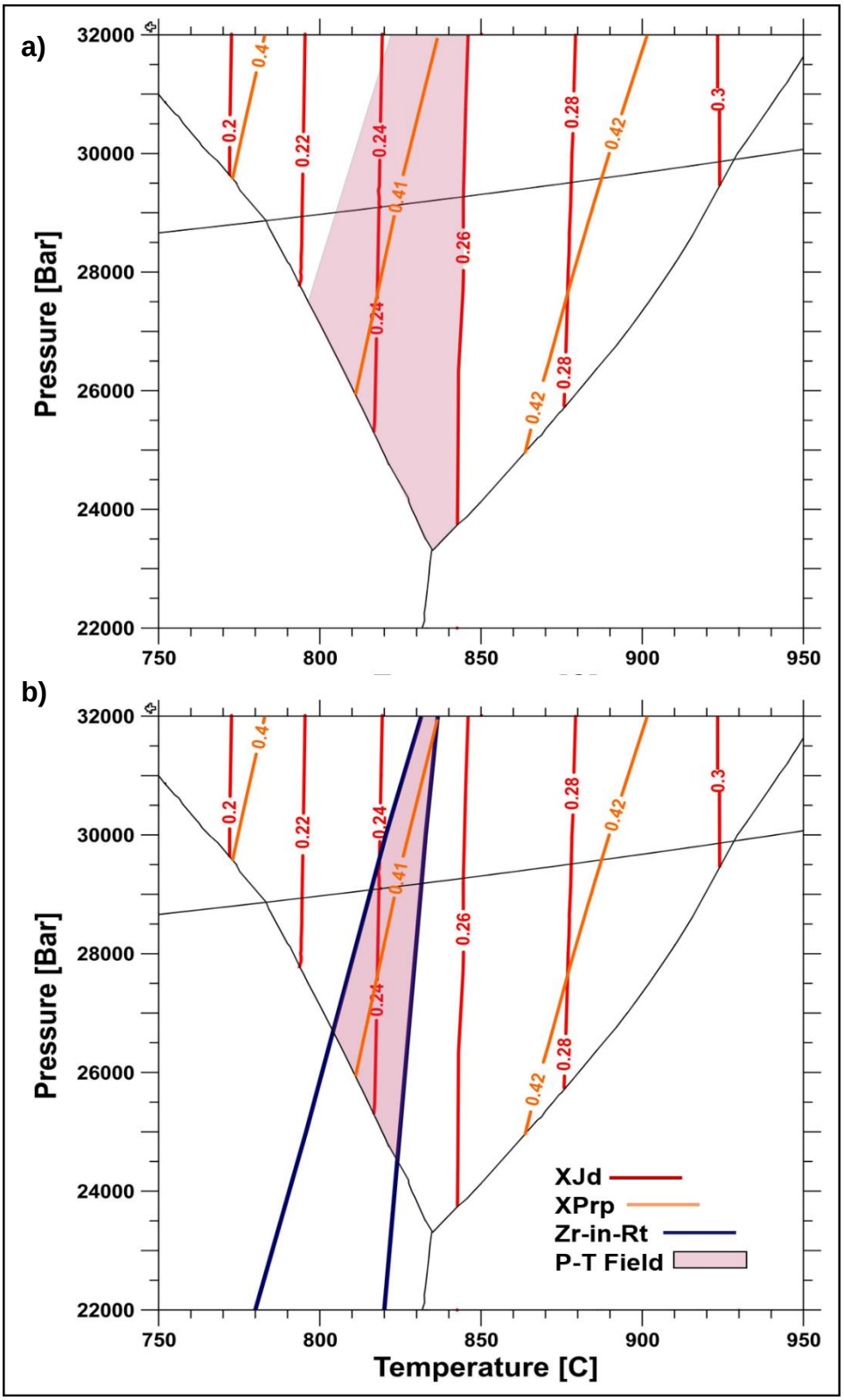

Figure 5.9. a) Measured XJd and XPrp overlap model isopleths at 800-840 °C and ca. 24-32 kb. b) Addition of Zr-in-rutile isopleths narrows the P-T range to 800-820 °C and ca. 25-32 kb.

5.5 P-T Results Summarised by Sample

5.5.1 CB15-19

For sample CB15-19, results from conventional Fe-Mg exchange thermometry overlap in the range 850-910 °C at 30 kb ($Fe^{2+} = Fe_{total}$), with garnet-clinopyroxene thermometry giving significantly lower T (400-570°C at 30 kb) calculated using Fe^{3+} values. These results can be interpreted as maxima and minima, respectively, but given the uncertainties involved, the data cannot be considered robust. This problem is discussed further in Chapter 6. In contrast, minor and trace element thermometers, based on Ti-in-biotite and Zr-in-rutile data, are not affected by Fe^{2+}/Fe^{3+} issues and appear to be less susceptible to retrogression. Data from these thermometers range from 716-783 °C and 781-820 °C, respectively, at 20 kb, and 832-910 °C and 763-868 °C at 30 kb. Equilibrium phase diagram calculations using Theriak-Domino (Section 5.4) indicate that the observed assemblage grt+omph+opx+bt+ rt+qz/cs+H_2O is stable over a very broad P-T range (Figure 5.7), with T of 780-930°C at the α-qz-cs transition, 29-30 kb. Within this broad range, model isopleths for XJd and XPrp overlap with analytical data from this sample in the range 800-840 °C and 24-32 kb (Figure 5.8). In combination, trace-element thermometry and Theriak-Domino results overlap in the range 800-820 °C and 25-32 kb, which is considered the best P-T estimate for sample CB15-19 (Figure 5.9).

5.5.2 CB15-70

For sample CB15-70, garnet-clinopyroxene thermometry yielded T results of 867-908 °C at 20 kb and 975-988 °C at 30 kb (Fe^{2+} = Fe total) and 523-617 °C at 20 kb, and 587-678 °C at 30 kb using Fe^{3+} values. These results do not overlap with the other Fe-Mg exchange thermometer results. The garnet-biotite and garnet-orthopyroxene thermometers yield a T range of 744-783 °C at 20 kb and 779-840 °C at 30 kb. Minor and trace element thermometers, Ti-in-biotite and Zr-in-rutile, gave a range in T of 735-817 °C and 827-864 °C at 20 and 30 kb, respectively.

5.5.3 CB15-44

Garnet-clinopyroxene thermometry yielded a T range of 858-869 °C at 20 kb and 916-928 °C at 30 kb ($Fe^{2+} = Fe_{total}$), and 649-709 °C at 20 kb and 696-759 °C at 30 kb when using calculated Fe^{3+} values. Orthopyroxene in this sample does not occur as inclusions in garnet and biotite is typically situated within amphibole inclusions in garnet, therefore garnet-biotite and

garnet-orthopyroxene thermometry were not used to calculated temperature in CB15-44. Zr-in-rutile thermometry yielded a T range of 695-749 °C at 20 kb and 735-792 °C at 30 kb.

Chapter 6: Discussion

6.1 Introduction

The results of the petrographic observations, conventional thermobarometry, and thermodynamic modelling presented in the previous chapters have been used to interpret the peak metamorphic conditions (i.e. T_{max} and $P@T_{max}$) for the eclogite samples from the Nordøyane domain. The mineralogical and textural variation across samples was used to assess whether the sample had maintained equilibrium during isothermal decompression along the retrograde metamorphic path, and mineral pairs that were interpreted to be in equilibrium were used in conventional thermobarometry calculations. Theriak-Domino, a thermodynamic modelling program (De Capitani and Petrakakis, 2010), was used with the bulk composition of sample CB15-19 in order to constrain the P-T estimates independent of conventional thermobarometry. The following chapter will discuss the P-T results in light of the reliability of the data and the effects of retrogression on the samples.

6.2 Assessment of P-T Estimates

6.2.1 P-T Range

The peak temperature estimates and the pressures at these peak temperatures (T_{max} and $P@T_{max}$) appear to be within the range of previously reported P-T estimates for the Nordøyane domain (Terry et al., 2000; Carswell et al., 2006; Butler et al., 2013). Chapter 5 details the difference in T results when using Fe^{2+} vs. Fe^{3+} and a summary of the reliable P-T results for each sample is presented in Chapter 5.5. The discrepancies in T using Fe^{2+} or Fe^{3+} with the garnet-clinopyroxene thermometer, a difference of ca. 200-300 °C, indicates that this method is unreliable for calculating T estimates for these eclogites. Although this discrepancy is not observed when using the garnet-biotite and garnet-orthopyroxene Fe-Mg exchange thermometers, T results from trace and minor element thermometers, Ti-in-biotite and Zr-in-rutile, are regarded as the most reliable as they appear less susceptible to retrogression. For sample CB15-19, the trace and minor element thermometers overlap in a T range of 781-868 °C between 20-30 kb. Using thermodynamic modelling (Chapter 5.4), the equilibrium diagram predicted that the observed mineral assemblage of grt+omph+opx+bt+rt+qz/cs+H_2O occupies a triangular region at P>23 kb and T 780 °C to 930 °C at the quartz-coesite reaction boundary. The

isopleths of XJd and XPrp for omphacite and garnet respectively plot in a P-T field of 750-950 °C at 23-32 kb, which is consistent with the mineral data collected via EMP (Figure 5.8). The observed XJd and XPrp data overlap in a field between ca. 800-840 °C and ca. 24-32 kb (Figure 5.9a). Superimposing the Zr-in-rutile isopleths narrows the P-T range to ca. 800-820 °C and ca. 25-32 kb (Figure 5.9b), which is interpreted to be the best estimate of the P-T conditions experienced by sample CB15-19.

Peak P-T conditions recorded in sample CB15-70 are like those in CB15-19, however, the garnet-clinopyroxene thermometer produced T > 900 °C. This is regarded as unrealistic as CB15-70 preserves greater amphibolite-facies overprinting than CB15-19. The other Fe-Mg thermometers overlap in a T range of 744-840 °C for 20-30 kb, similar to the T range from the Zr-in-rutile and Ti-in-biotite thermometers, 735-864 °C for 20-30 kb. Thermodynamic modelling was only done with bulk composition CB15-19, so the most reliable T range for CB15-70 is 735-864 °C, based on the minor and trace element thermometers.

For sample CB15-44, the garnet-clinopyroxene thermometer yielded T in the range of 649-759 °C for 20-30 kb when using Fe^{3+} values. This partially overlaps with the T range of 695-792 °C from the Zr-in-rutile thermometer. This is the lowest range in temperature from any of the samples, and probably reflects the extensive hydration experienced by sample CB15-44. With a reported uncertainty of ± 50 °C for the garnet-clinopyroxene, Ti-in-biotite, Zr-in-rutile thermometers, ± 25 °C for the garnet-biotite thermometer, and ± 40 °C for the garnet-orthopyroxene thermometer (Ravna, 2000; Wu and Chen, 2015; Tomkins et al., 2007; Holdaway, 2000; Harley, 1984), many of these T estimates are within error of each other.

Because the rocks comprise mineral assemblages dominated by omphacite and garnet, thermometry based on Fe-Mg exchange between these minerals was the primary method to calculate the T_{max} and $P@T_{max}$. Previous work has documented P-T conditions in the Nordøyane domain of 750-850 °C between 3-5 GPa (Terry et al., 2000b; Cuthbert et al., 2000; Butler et al., 2013). T estimates above 900 °C at 30 kb (908 °C for CB15-19; 988 °C for CB15-70; 928 °C for CB15-44) have yet to be documented from eclogite in the study area, and thus the garnet-clinopyroxene T results at 30 kb obtained from these samples are higher than expected. In contrast, the results based on Zr-in-rutile and Ti-in-biotite, and thermodynamic modelling for CB15-19, are in good agreement with previous results.

6.2.2 Retrograde Exchange

The assumption that the mineral assemblage present in the rocks represents equilibrium is the most important concern when assessing the P-T results produced by conventional thermobarometry (Powell and Holland, 2008). Initially, the texture and observed mineral assemblage in CB15-19 suggested that peak conditions might be preserved, a reason why it was a focus of this work. Because of the eclogite-facies mineral assemblage, the homogeneity of the garnet grains, the well-preserved, idioblastic inclusions within garnet, and the lack of intergranular symplectite texture compared with other studied samples, it seemed likely that CB15-19 would yield the most reliable peak P-T results. While the observed mineral assemblage appears to be consistent with the predicted UHP assemblage from Theriak-Domino modelling (Chapter 5.4), it is clear from the Fe-Mg thermometry results (calculated for Fe3+) that the mineral compositions preserved in the samples do not reflect equilibrium. A possible explanation for this is that while the garnets appear homogenous (i.e. lack of zoning in garnet cores; only slight enrichment of Mn towards the rims), the entire grains may have been affected by diffusion during retrogression. The following discussion focuses on sample CB15-19 because its bulk composition was used to create the phase diagram (Figure 5.7) that provides the best independent constraints on P-T conditions. While the thermometers yielded a T range of ca. 700-910 °C (Chapter 5.5), thermodynamic modelling results indicate that these T results are less robust than expected.

The interpretation that the measured mineral compositions in CB15-19 reflect peak P-T conditions is contradicted by the isopleths for observed mole fractions (Figure 5.8). The predicted mole fraction isopleths (i.e. XGrs, XDi, XPhl, XEns) within the P-T range of interest are inconsistent with the data from the EMP analyses. For example, the model predicts XGrs = 0.065-0.07 in the relevant P-T range (Figure 5.8), while observed XGrs is 0.09-0.11. The other listed mole fractions follow this trend. A comparison of observed and predicted mineral compositions shows that measured compositions are compatible with lower T and/or P conditions than suggested by the observed assemblage. Only the XJd and XPrp isopleths produced by Theriak-Domino are consistent with EMP analyses of garnet and omphacite (Figure 5.9a). The contrast between the thermobarometry P-T results and the Theriak-Domino model results suggests that the mineral compositions used to estimate peak P-T conditions (garnet cores and associated inclusions) were more extensively affected by retrograde diffusion than initially

thought.

The extent of retrograde diffusive exchange of Fe-Mg depends on the temperature, the grain size, and the rate of cooling (Borinski et al., 2012; Li et al., 2018). Eclogite-facies metamorphism in the domain has been dated at 415-410 Ma (Terry et al., 2000; Krogh et al., 2011) and amphibolite-facies pegmatite bodies between eclogite boudins have been dated at ca. 395 Ma (Krogh et al., 2011). Butler and Jamieson (submitted) concluded that scapolite pegmatites in the study area crystallised at 750-800 °C and ca. 10 kb, while P-T estimates from amphibolite-facies assemblages overprinting eclogite suggest a range of 750-825 °C and ca. 10-12 kb (Terry and Robinson, 2003; Butler et al., 2013). This suggests a period of ca. 15-20 Ma (Krogh et al., 2011) between peak metamorphic conditions (ca. 750-850 °C and ca. 3-5 GPa; Terry et al., 2000b; Cuthbert et al., 2000; Butler et al., 2013) and amphibolite-facies conditions, during which these rocks remained at $T \geq 750$ °C. This appears to be ample time for diffusion to occur (Duchêne and Albarède, 1999; Borinski et al., 2012).

Typically, diffusional zoning in garnet does not penetrate to the core and is present mostly in the outer core and rim (Borinski et al., 2012). Garnet cores typically preserve their peak metamorphic compositions during rapid cooling at rates greater than 100 °C/My (Borinski et al., 2012). In this case, Fe-Mg exchange thermometry applied to garnet and coexisting mineral inclusions in the core would yield P-T results that reflect the peak metamorphic conditions. However, slow cooling from $T > 750$ °C at a rate of ca. 1-2 °C/My can reset the composition of garnet cores that are several millimetres across (Borinski et al., 2012). The latter is more consistent with the exhumation history of the Nordøyane domain. It is likely that during the prolonged period during which the eclogite samples remained at high temperatures (750-800 °C), efficient diffusion affected garnet and clinopyroxene compositions, resulting in unreliable temperature estimates using Fe-Mg exchange thermometry.

Although Ca in garnet is generally considered to have low diffusion rates, the low Ca content of garnet compared with that of omphacite would have made XGrs susceptible to exchange with clinopyroxene in the inclusions and the matrix. This may explain the discrepancy between the observed XGrs data and the predicted model isopleths, which suggests that higher XGrs trends towards lower P and T (Figure 5.8). In contrast, relatively immobile elements such as Zr (in rutile) and Ti (in biotite) within Zr- and Ti-poor garnet appear to have retained their peak compositions. Fe-Mg diffusion during retrogression would have affected smaller inclusions

of biotite, omphacite, and orthopyroxene more than the coarser-grained Fe-Mg-rich host garnet. This can explain why the observed XEns, XDi, and XPhl data do not plot in the P-T field predicted by Theriak-Domino (Figure 5.8).

The difference between thermobarometry results and thermodynamic modelling results, attributed to grain-scale diffusion during retrogression, suggests that Fe-Mg exchange thermometry results are less robust than trace and minor element thermometry. Temperature results from these thermometers, paired with the equilibrium diagram, are regarded as most reliable. In combination they yield a T range of 800-820 °C at 25-32 kb for sample CB15-19 (Chapter 5.5), which is considered the best P-T estimate for this sample. If the Zr-in-rutile thermometer results for CB15-70 and CB15-44 are also reliable, a T range of 782-864 and 695-792 °C ± 50 °C at 20-30 kb is estimated for these samples, respectively. However, the corresponding pressure cannot be constrained independently for these samples.

6.3 Implications

6.3.1 Melting

In order to test the hypothesis that the eclogites and their host rocks reached P-T conditions where UHP melting is possible, P-T conditions determined from the overlap among XJd, XPrp, and Zr-in-rutile isopleths (Figure 5.9b) were superimposed on a P-T diagram showing the melting curves for various crustal compositions determined by previous experimental studies (Figure 6.1) From this diagram, the P-T conditions overlap with the field of fluid-present UHP melting, that is, between the fluid-saturated melting curves (solid lines) and the dehydration melting curves (dashed lines). Fluid-present melting is consistent with the Theriak-Domino prediction that a small amount of H2O (≤ 1 vol%) is present in the P-T field corresponding to the mineral assemblage of CB15-19.

While the P-T field partially overlaps with the field where fluid-present melting is possible for basaltic rocks, no in situ melting is observed in the eclogite samples. It is possible that the migmatitic orthogneiss host rocks melted at these peak conditions, however, any evidence of in situ melting has been obscured during late-stage decompression melting and subsequent high strain. Bryden and Jamieson (in press) suggest that an externally derived fluid may have infiltrated the high T region of the subducting slab and triggered partial melting of the Baltican crust based on $\delta^{34}S$ and $\delta^{13}C$ signatures of Nordøyane scapolites. However, the timing of this event (i.e. before or during exhumation) could not be constrained (Bryden and Jamieson,

in press). The P-T conditions indicate that melting of the host rocks in the presence of a fluid was possible during peak metamorphism. In the absence of unambiguous evidence for the presence of a fluid at peak P-T conditions, or on the timing of fluid infiltration, the question of whether partial melting triggered the exhumation of the WGR remains unresolved.

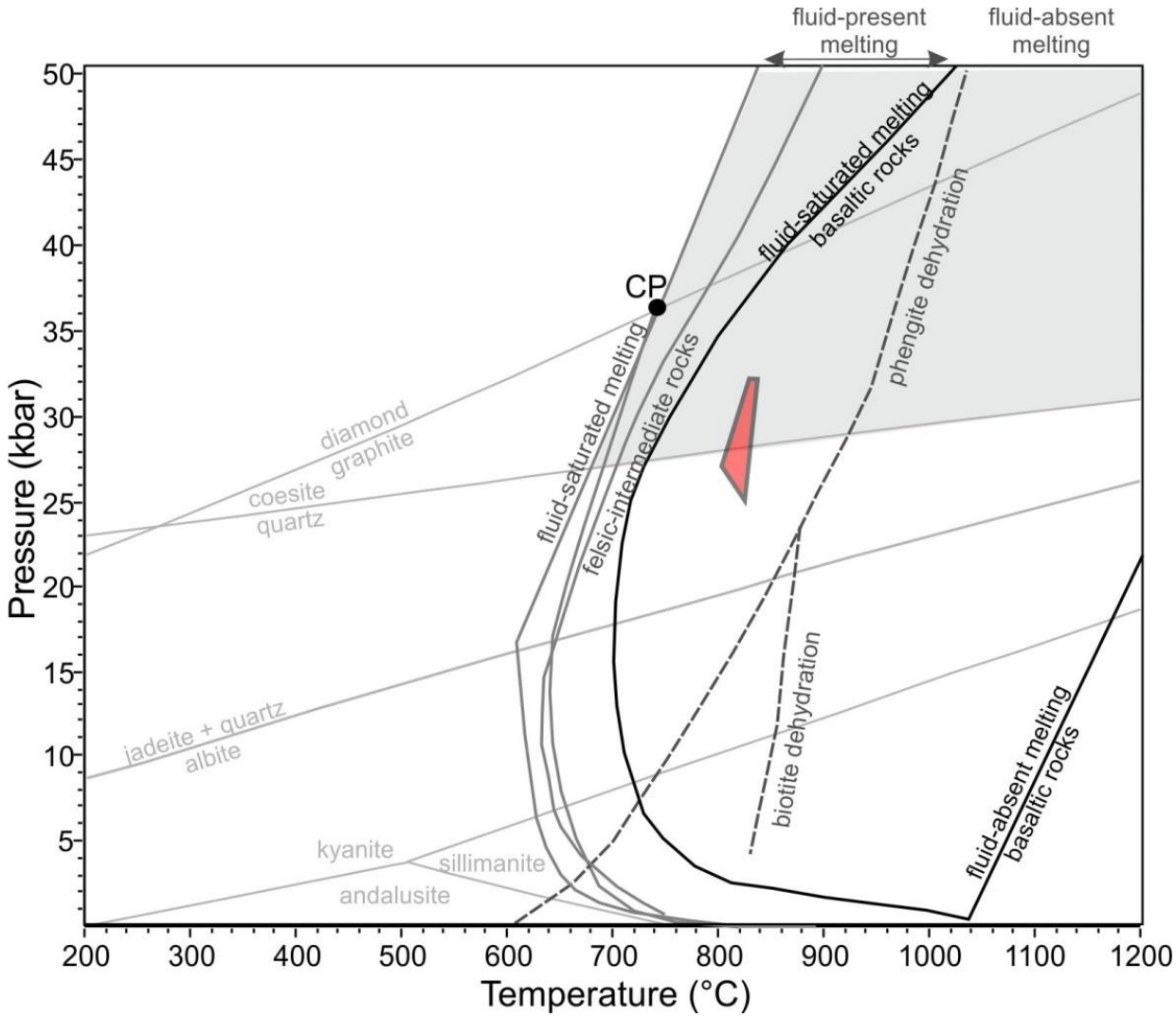

Figure 6.1: In red, the field defined by the overlap in XJd and XPrp observed data and the superimposed Zr-in-Rutile isopleths produce a field between 800-820°C and 25-32 kb, which partially overlaps with the field of fluid-present-UHP melting. P-T diagram shows melting curves for various crustal compositions (Kessel et al. 2005, Patiño Douce 2005, Hermann & Spandler 2008, Auzanneau et al. 2006). Reference reaction curves (light grey) calculated using WinTWQ (Berman, 2007); CP= critical point, where distinction between melt and fluid disappears (Hermann & Rubatto, 2014)

6.3.2 Tectonics and Exhumation

The WGR was affected by HP-UHP metamorphism as a result of burial of the Baltican margin during the Scandian phase of the Caledonian orogeny beneath an already thick and hot orogen which had accreted over a long period of plate convergence (e.g., Roberts, 2003; Hacker and Gans, 2005; Corfu et al., 2014). Many mechanisms responsible for the exhumation of the region have been proposed (Chapter 1, 2). This study was designed to test the hypothesis that partial melting at UHP conditions may have been the trigger for exhumation (Labrousse et al., 2011; Ganzhorn et al., 2014) by determining whether the rocks in the study area were hot enough to melt at those conditions.

Butler et al. (2015) presented geodynamic models for the WGR based on the hypothesis that the Baltican margin remained coupled to the subducting slab at UHP conditions, inhibiting exhumation. The models suggested that exhumation of the terrane was a result of extension during plate divergence (Fossen, 1992; Butler et al., 2015). Models that involve plate divergence as the main exhumation mechanism are compatible with a broad range of observations and data, such as the lack of regional-scale thrust faults separating UHP rocks in the hangingwall from the lower P rocks in the footwall and the timing and P-T conditions of metamorphism and cooling across the region (Hacker et al., 2010; Butler et al., 2015). Before the Scandian orogeny, the Baltican crust was already strong as it underwent Proterozoic granulite-facies metamorphism (Bingen et al., 2008; Spencer et al., 2013) leaving it dehydrated, which suggests that the region could have been exhumed as a coherent slab (Butler et al., 2015). In contrast, models incorporating partial melting at UHP conditions (Figure 6.2) showed that the crust must be weak in order to decouple from the subducting slab and rise as an independent plume. Butler et al. (2015) concluded that models involving plate divergence are more compatible with the data than models incorporating partial melting as the dominant process driving exhumation.

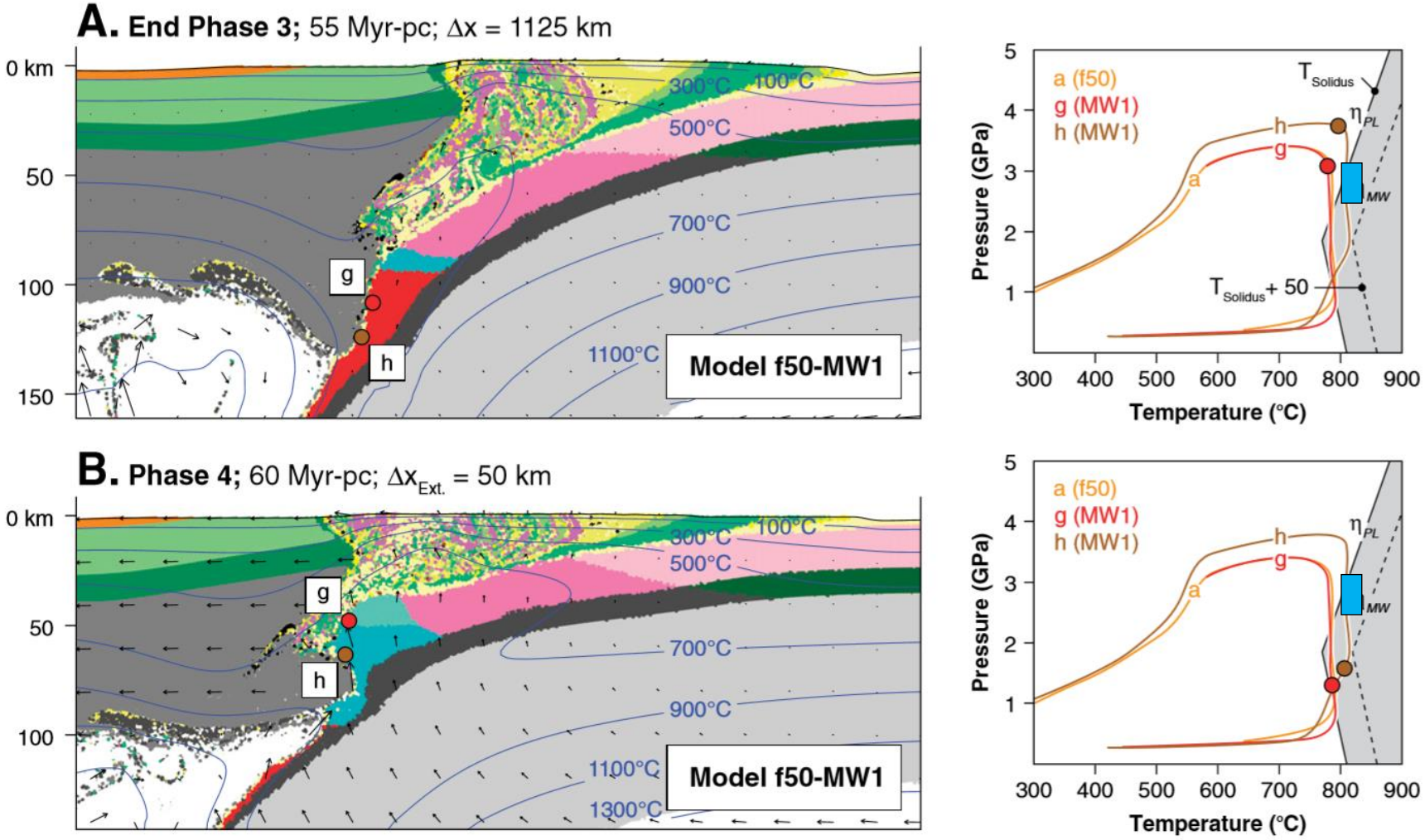

Figure 6.2. Comparison of tectonic evolution (left) and equivalent P-T paths from model f50-MW1 showing the effects of partial melting (right) (Butler et al., 2015). Gray area corresponds (right) to region of melt weakening. Model P-T-t paths for tracked particles g and h are shown in panels on right. The blue rectangle corresponds to the T results for sample CB15-19 constrained by the Zr-in-rutile thermometer and Theriak-Domino modelling (800-820 °C, ca. 25-32 kb).

The model incorporating extensive melting at peak conditions (Figure 6.2) tracks the P-T paths of particles during burial, heating and exhumation. The model suggests that T > 800 °C at 3 GPa is required for the particles to enter the partial melting field before isothermal decompression leads to the extensive decompression melting (Butler et al., 2015). Butler et al. (2015) suggested that because the tracked particles only enter the partial melting field during exhumation at P < 25 kb, that partial melting at UHP conditions is not possible under the model with a minimum water content. In addition, the study concluded that exhumation triggered by UHP melting was less likely than exhumation facilitated by extension during plate divergence because the style of melt-driven exhumation is not what is observed in the region (Butler et al., 2015). However, the P-T data from CB15-19 indicate that the sample reached a T of 800-820 °C and 25-32 kb (Figure 6.2). That would place sample CB15-19 in the field of partial melting along the model P-T-t path suggested by the model. Butler et al. (2015) also included a model with a greater water content than the one discussed, which would certainly place sample CB15-19 in the field where partial melting is possible.

Chapter 7: Conclusions and Recommendations for Further Work

7.1 Conclusions

- Sample CB15-19 is a massive eclogite comprising a peak mineral assemblage of garnet + omphacite + biotite + orthopyroxene + rutile. Sample CB15-70 comprises a similar assemblage and displays compositional banding. Sample CB15-44 is very coarse-grained, extensively hydrated, and lacks orthopyroxene.
- Thermobarometry and thermodynamic modelling methods were used to calculate P-T conditions for eclogite sample CB15-19 and thermobarometry for samples CB15-70 and CB15-44, based on the peak mineral assemblage of garnet + omphacite + biotite + orthopyroxene + rutile.
- Calibrated thermometers based on Fe-Mg exchange reactions, specifically between garnet and clinopyroxene, proved to be unreliable for calculating P-T estimates. This problem reflects two main factors: Fe^{3+} and grain scale diffusion during retrogression. Trace and minor element thermometers, Zr-in-rutile and Ti-in-biotite, produced more robust P-T results.
- For CB15-19 and CB15-70, the Zr-in-rutile and Ti-in-biotite thermometers yielded a T range of 781-868 °C and 735-864 °C, respectively, for 20-30 kb. The Zr-in-rutile thermometer gave a T range of 695-792 °C for CB15-44.
- Thermodynamic modelling of bulk composition CB15-19 produced a broad P-T range for the observed mineral assemblage of 780-930 °C at P > 23 kb. Isopleths of XJd, XPrp and Zr-in-rutile narrowed this field to ca. 800-820 °C and ca. 23-32 kb. These are interpreted as the best estimate of the P-T conditions (T_{max} and $P@T_{max}$) experienced by CB15-19.
- P-T conditions from CB15-19 overlap with the field where UHP melting is possible in the presence of a fluid for a range of bulk compositions.

7.2 Recommendations for Further Work

The results of this study indicate that the T_{max} and $P@T_{max}$ conditions recorded in the eclogite samples overlap in the range where fluid-present UHP melting is possible for the

intermediate host rocks. However, the study cannot conclude that melting at UHP conditions assisted in the exhumation of the WGR because peak P conditions were not determined, and there was no evidence for *in situ* melting or fluid infiltration at peak conditions preserved in the eclogites. The hypothesis that partial melting assisted in the exhumation process could be strengthened by independent P constraints for the samples. The mineral assemblages present in the studied samples proved unsuitable for independent P determinations (e.g., quartz-in-garnet and phengite barometry). While the mineralogy reflects the bulk composition, more samples from the study areas could be analysed

T constraints for samples CB15-70 and CB15-44 could be achieved through thermodynamic modelling with their bulk compositions. The Ti-in-zircon thermometer could be used if zircons in all samples were analysed by laser ablation. This study did not produce a P-T-t path for any of the samples, which could be completed with more detailed analysis of the retrograde mineral assemblage present in the symplectite. A P-T-t path of these samples would help constrain the P-T conditions during decompression. Geochronology of zircons in the eclogites could constrain the timing of the eclogite-facies metamorphism.

References

Andersen, T.B. 1998. Extensional tectonics in the Caledonides of southern Norway, an overview. Tectonophysics **285:** 333–351.

Auzanneau, E., Vielzeuf, E., Schmidt, M.W. 2006. Experimental evidene of decompression melting during exhumation of subducted continental crust. Contributions to Mineralogy and Petrology. **152:** 125-148.

Berman, R. G. 1988. Internally consistent thermodynamic data for minerals in the system Na_2O-K_2O-CaO-MgO-FeO-Fe_2O_3-Al_2O_3-SiO_2-TiO_2-H_2O-CO_2. Journal of Petrology. **29:** 445-522.

Berman, R.G., Aranovich, L.Y. 1996. Optimized standard state and mixing properties of minerals: I. Model calibration for oivine, orthopyroxene, cordierite, garnet, and ilmenite in the system FeO-MgO-CaO-Al_2O_3-SiO_2-TiO_2. Contributions to Mineralogy and Petrology. **126**: 1-24

Berman, R.G. 2007. winTWQ (version 2.3): a software package for performing internally-consistent thermobarometric calculations. Geological Survey of Canada. open file 5462: 41

Bhattacharya, A. C., Spiering, B., Sen, S. K., Natarajan, R. and Mazumdar, A. C. 1990. Compositional characterics and phase equlibria in manganiferous iron formations from a high grade terrain near Satnuru, Karnataka, India. Journal of Metamorphic Geology, **8:** 525-538

Bingen, B., Andersson, J., Söderlund, U., and Möller, C. 2008. The Mesoproterozoic in the Nordic countries. Episodes, **31**: 29–34. doi:10.18814/epiiugs/2008/v31i1/005.

Borinski, S.A., Hoppe, U., Chakraborty, S., Ganguly, J., and Bhowmik, S.K. 2012. Multicomponent diffusion in garnets I: General theoretical considerations and experimental data for Fe-Mg systems. Contributions to Mineralogy and Petrology, **164**: 571–586. doi:10.1007/s00410-012-0758-0.

Bryden, C.D. 2017. Stable isotope chemistry and geochronolgy of scapolite-bearing pegmatites in Nordøyane, Western Gneiss Region, Norway: a monitor for the role of fluids in (ultra)-high pressure partial melting. Unpublished MSc thesis, Dalhousie University, Halifax, NS, Canada, 290 pp.

Bryden, C.D., and Jamieson, R.A. 2020. Scapolite pegmatite from the Nordøyane domain,

Western Gneiss Region , Norway : Partial melting driven by infiltration of mantle-derived fluid. Lithos, accepted 19 April 2020. doi: 10.1016/j.lit.hos.2020.105546

Butler, J.P., Beaumont, C., and Jamieson, R.A. 2015. Paradigm lost: Buoyancy thwarted by the strength of the western gneiss region (ultra)high-pressure terrane, Norway. Lithosphere, **7:** 379–407. doi:10.1130/L426.1.

Butler, J.P., Jamieson, R.A., Steenkamp, H.M., and Robinson, P. 2013. Discovery of coesite-eclogite from the Nordøyane UHP domain, Western Gneiss Region, Norway: Field relations, metamorphic history, and tectonic significance. Journal of Metamorphic Geology, **31**: 147–163. doi:10.1111/jmg.12004.

Butler, J.P., Jamieson, R.A., Dunning, G.R., Pecha, M., Robinson, P., Steenkamp, H.M. 2018. Timing of metamorphism and exhumation in the Nordøyane ultra-high-pressure domain, Western Gneiss Region, Norway: New constrains from complementary CA-ID-TIMS and LA-MC-ICP-MS geochronology. Lithos. 310-311, 153-170. doi:10.1016/j.lithos.2018.04.006

De Capitani, C., and Petrakakis, K. 2010. The computation of equilibrium assemblage diagrams with Theriak/Domino software. American Mineralogist, **95**: 1006–1016. doi:10.2138/am.2010.3354.

Carswell, D.A., van Roermund, H.L.M., and Wiggers de Vries, D.F. 2006. Scandian ultrahigh-pressure metamorphism of proterozoic basement rocks on Fjørtoft and Otrøy, Western Gneiss Region, Norway. International Geology Review, **48**: 957–977. doi:10.2747/0020-6814.48.11.957.

Chopin, C. 1984. Coesite and pure pyrope in high-grade blueschists of the Western Alps: a first record and some consequences. Contributions to Mineralogy and Petrology, **86**: 107–118. doi:10.1007/BF00381838.

Corfu, F., Andersen, T.B., Gasser, D. 2014. The Scandinavian Caledonides: Main features, conceptual advances and critical questions. in: Corfu, F., Gasser, D., Chew, D.M. (Eds.), New Perspectives on the Caledonides of Scandinavia and Related Areas, Geological Society of London, Special Publication 390, 9-43, doi:10.1144/SP390.25.

Cuthbert, S.J., Carswell, D.A., Krogh-Ravna, E.J., and Wain, A. 2000. Eclogites and eclogites in the Western Gneiss region, Norwegian Caledonides. Lithos, **52**: 165–195.

doi:10.1016/S0024-4937(99)00090-0.

Dobrzhinetskaya, L.F., Eide, E.A., Larsen, R.B., Sturt, B.A., Trønnes, R.G., Smith, D.C., Taylor, W.R., Psoukhova, T.V. 1995. Microdiamond in high-grade metamorphic rocks of the Western Gneiss region, Norway. Geology, **23**: 597–600. doi:10.1130/0091-7613(1995)023

Duchêne, S., and Albarède, F. 1999. Simulated garnet-clinopyroxene geothermometry of eclogites. Contributions to Mineralogy and Petrology, **135**: 75–91. doi:10.1007/s004100050499.

Ellis, D.J., and Green, D.H. 1979. An experimental study of the effect of Ca upon garnet-clinopyroxene Fe-Mg exchange equilibria. Contributions to Mineralogy and Petrology, **71**: 13–22. doi:10.1007/BF00371878.

Fossen, H. 2000. Extensional tectonics in the Caledonides: Synorogenic or postorogenic. Tectonics, **19**: 213–224. doi:10.1029/1999TC900066.

Ganzhorn, A.C., Labrousse, L., Prouteau, G., Leroy, C., Vrijmoed, J.C., Andersen, T.B., and Arbaret, L. 2014. Structural, petrological and chemical analysis of syn-kinematic migmatites: Insights from the Western Gneiss Region, Norway. Journal of Metamorphic Geology, **32**: 647–673. doi:10.1111/jmg.12084.

Gordon, S.M., Whitney, D.L., Teyssier, C., and Fossen, H., 2013, U-Pb dates and trace-element geochemistry of zircon from migmatite, Western Gneiss Region, Norway: Significance for history of partial melting in continental subduction: Lithos, **170:** 35–53. doi:10 .1016/j .lithos .2013 .02 .003.

Hacker, B.R., Andersen, T.B., Johnston, S., Kylander-Clark, A.R.C., Peterman, E.M., Walsh, E.O., and Young, D. 2010. High-temperature deformation during continental-margin subduction & exhumation: The ultrahigh-pressure Western Gneiss Region of Norway. Tectonophysics, **480**: 149–171. doi:10.1016/j.tecto.2009.08.012.

Hacker, B.R., and Gans, P.B. 2005. Continental collisions and the creation of ultrahigh-pressure terranes: Petrology and thermochronology of nappes in the central Scandinavian Caledonides. Bulletin of the Geological Society of America, **117**: 117–134. doi:10.1130/B25549.1.

Harley, S.L. 1984. An experimental study of the partitioning of Fe and Mg between garnet and orthopyroxene. Contributions to Mineralogy and Petrology, **86**: 359–373.

doi:10.1007/BF01187140.

Herman, J., and Spandler, C.J. 2008. Sediment melts at sub-arc depths: an experimental study. Journal of Petrology. **49.4:** 717-740

Hermann, J., Rubatto, D. 2014. Subduction of continental crust to mantle depths: Geochemistry of ultrahigh-pressure rocks. Treatise on Geochemistry. **4:** 309-340. doi:10.1016/B978-0-08-095975-7.00309-0.

Hilchie, L., Jamieson, R.A., Bryden, C.D., Terry, M., & Chapman, G.G. (2019) Secrets of the Temple of Doom – new coesite discoveries in western Norway. Atlantic Geoscience Society, Fredericton, February 2019; Atlantic Geology. **55**: 179-180.

Holdaway, M.J. 2000. Application of new ecperimental and garnet margules data to the garnet-biotite geothermometers. Am. Mineral. **85:** 881-892.

Johnston, S., Hacker, B.R., and Ducea, M.N. 2007. Exhumation of ultrahigh-pressure rocks beneath the Hornelen segment of the Nordfjord-Sogn Detachment Zone, western Norway. Bulletin of the Geological Society of America, **119**: 1232–1248. doi:10.1130/B26172.1.

Kessel, R., Ulmer, P., Pettke, T., Schmidt, M.W., Thompson, A.B. 2005. The water-basalt system at 4 to 6 GPa: Phase relations and second critical endpoint in a K-free eclogite at 700 to 1400 °C. Earth and Planetary Science Letters. **237:** 873-892.

Kleeman, U., Reinhardt, J. 1994. Garnet-biotite thermometry revisited: The effect of AlVI and Ti in biotite. European Journal of Mineralogy. **6:** 925-941. doi:10.1127/ejm/6/6/0925

Krabbendam, M., Dewey, J.F., 1998. Exhumation of UHP rocks by transtension in the Western Gneiss Region, Scandinavian Caledonides. Geol. Soc. Lond., Spec. Publ. **135:** 159–181.

Krogh Ravna, E.J. 1988. The garnet-clinopyroxene Fe-Mg geothermometer - a reinterpretation of existing experimental data. Contributions to Mineralogy and Petrology, **99**: 44–48. doi:10.1007/BF00399364.

Krogh Ravna. E.J. 2000. The garnet – clinopyroxene Fe^{2+}-Mg geothermometer : an updated calibration. Journal of Metamorphic Geology, **18**: 211–219.

Krogh, T.E., Kamo, S.L., Robinson, P., Terry, M.P., and Kwok, K. 2011. U-Pb zircon geochronology of eclogites from the Scandian Orogen, Northern Western Gneiss Region, Norway: 14-20 million years between eclogite crystallization and return to amphibolite-facies conditions. Canadian Journal of Earth Sciences, **48**: 441–472. doi:10.1139/E10-076.

Kylander-Clark, A.R.C., Hacker, B.R., Johnson, C.M., Beard, B.L., Mahlen, N.J., and Lapen, T.J. 2007. Coupled Lu-Hf and Sm-Nd geochronology constrains prograde and exhumation histories of high- and ultrahigh-pressure eclogites from western Norway. Chemical Geology, **242**: 137–154. doi:10.1016/j.chemgeo.2007.03.006.

Labrousse, L., Prouteau, G., and Ganzhorn, A.C. 2011. Continental exhumation triggered by partial melting at ultrahigh pressure. Geology, **39**: 1171–1174. doi:10.1130/G32316.1.

Lanari, P., and Duesterhoeft, E. 2019. Modeling metamorphic rocks using equilibrium thermodynamics and internally consistent databases: Past achievements, problems and perspectives. Journal of Petrology, **60**: 19–56. doi:10.1093/petrology/egy105.

Li, B., Ge, J., and Zhang, B. 2018. Diffusion in garnet: a review. Acta Geochimica**, 37:** 19–31. doi:10.1007/s11631-017-0187-x.

Nakamura, D. 2009. A new formulation of garnet-clinopyroxene geothermometer based on accumulation and statistcal analysis of a large experimental data set. J Metamorphic Geology. **27:** 495-508

Patiño Douce, A.E. 2005. Vapor-absent melting of tonalite at 15-32 kbar. Journal of Petrology. **46:** 275-290.

Powell, R., and Holland, T.J.B. 1998. An internally consistent thermodynamic data set for phases of petrological interest. Journal of Metamorphic Geology. **16:** 309-343.

Powell, R., and Holland, T.J.B. 2008. On thermobarometry. Journal of Metamorphic Geology, **26**: 155–179. doi:10.1111/j.1525-1314.2007.00756.x.

Råheim, A., and Green, D.H. 1974. Experimental determination of the temperature and pressure dependence of the Fe-Mg partition coefficient for coexisting garnet and clinopyroxene. Contributions to Mineralogy and Petrology, **48**: 179–203. doi:10.1007/BF00383355.

Roberts, D., 2003. The Scandinavian Caledonides: Event chronology, palaeogeographic settings and likely modern analogues: Tectonophysics. **365**: 283-299. doi:10.1016/S0040-1951(03)00026-X.

Root, D.B., Hacker, B.R., Gans, P.B., Ducea, M.N., Eide, E.A., and Mosenfelder, J.L. 2005. Discrete ultrahigh-pressure domains in the Western Gneiss Region, Norway: Implications for formation and exhumation. Journal of Metamorphic Geology, **23**: 45–61. doi:10.1111/j.1525-1314.2005.00561.x.

Sawyer, E.W. 2008 Working with migmatites: Nomenclature for the constituent parts. in: Sawyer, E.W., Brown, M. (Eds.), Working with Migmatites. Mineralogical Association of Canada, Short Course 38, Quebec City, 1-28.

Smith, D.C. 1984. Coesite in clinopyroxene in the Caledonides and its implications for geodynamics. Nature, **310**: 641–644. doi:10.1038/310641a0.

Spear, F.S. 1993. Metamorphic Phase Equlibria and Pressure-Temperature-Time Paths. Mineralogical Society of America. Washington, D.C., USA.

Spencer, K.J., Hacker, B.R., Kylander-Clark, A.R.C., Andersen, T.B., Cottle, J.M., Stearns, M.A., Poletti, J.E., and Seward, G.G.E. 2013. Campaign-style titanite U-Pb dating by laser-ablation ICP: Implications for crustal flow, phase transformations and titanite closure. Chemical Geology, **341:** 84–101. doi:10.1016/j.chemgeo.2012.11.012.

Terry, M.P., and Robinson, P. 2003. Evolution of amphibolite-facies structural features and boundary conditions for deformation during exhumation of high- and ultrahigh-pressure rocks, Nordøyane, Western Gneiss Region, Norway. Tectonics, **22**: 1036 doi:10.1029/2001TC001349.

Terry, M.P., and Robinson, P. 2004. Geometry of eclogite-facies structural features: Implications for production and exhumation of ultrahigh-pressure and high-pressure rocks, Western Gneiss Region, Norway. Tectonics, **23**: 1–23. doi:10.1029/2002TC001401.

Terry, M.P., Robinson, P., and Krogh Ravna, E.J. 2000. Kyanite eclogite thermobarometry and evidence for thrusting of UHP over HP metamorphic rocks, Nordoyane, Western Gneiss Region, Norway. American Mineralogist, **85**: 1637–1650. doi:10.2138/am-2000-11-1207.

Tomkins, H.S., Powell, R., and Ellis, D.J. 2007. The pressure dependence of the zirconium-in-rutile thermometer. Journal of Metamorphic Geology, **25**: 703–713. doi:10.1111/j.1525-1314.2007.00724.x.

Tucker, R.D., Robinson, P., Solli, A., Gee, D.G., Thorsnes, T., Krogh, T.E., Nordgulen, Ø., and Bickford, M.E. 2004. Thrusting and extension in the Scandian hinterland, Norway: New U-Pb ages and tectonostratigraphic evidence. American Journal of Science, **304**: 477–532. doi:10.2475/ajs.304.6.477.

Wain, A. 1997. New evidence for coesite in eclogite and gneisses: Defining an ultrahigh-pressure province in the Western Gneiss region of Norway. Geology, **25**: 927–930.

doi:10.1130/0091-7613(1997)025

Watson, E.B., Wark, D.A., and Thomas, J.B. 2006. Crystallization thermometers for zircon and rutile. Contributions to Mineralogy and Petrology, **151**: 413–433. doi:10.1007/s00410-006-0068-5.

Wu, C.M., and Chen, H.X. 2015. Revised Ti-in-biotite geothermometer for ilmenite- or rutile-bearing crustal metapelites. Science Bulletin, **60**: 116–121. doi:10.1007/s11434-014-0674-y.

Yakymchuk, C. 2017. Applying phase equilibria modelling to metamorphic and geological processes: Recent developments and future potential. Geoscience Canada, **44**: 27–46. doi:10.12789/geocanj.2017.44.114.

Zack, T., Kronz, A., Foley, S.F., Rivers, T. 2002. Trace element abundances in rutiles from eclogites and associated garnet mica schists. Chem Geol. **184:** 97-122.

Zack, T., Moraes, R., and Kronz, A. 2004. Temperature dependence of Zr in rutile: Empirical calibration of a rutile thermometer. Contributions to Mineralogy and Petrology, **148**: 471–488. doi:10.1007/s00410-004-0617-8.